Journal of Medicinal Chemistry

Article

Development of Purine-Based Hydroxamic Acid Derivatives: Potent Histone Deacetylase Inhibitors with Marked in Vitro and in Vivo Antitumor Activities

Yong Chen, Xiaoyan Wang, Wei Xiang, Lin He, Minghai Tang, Fang Wang, Taijin Wang, Zhuang Yang, Yuyao Yi, Hairong Wang, Ting Niu, Li Zheng, Lei Lei, Xiaobin Li, Hang Song, and LiJuan Chen

J. Med. Chem., **Just Accepted Manuscript** • DOI: 10.1021/acs.jmedchem.6b00579 • Publication Date (Web): 17 May 2016

	University Song, Hang; Sichuan University, School of Chemical Engineering Chen, LiJuan; State Key Laboratory of Biotherapy, West China Medical School

Development of Purine-Based Hydroxamic Acid Derivatives: Potent Histone Deacetylase Inhibitors with Marked in Vitro and in Vivo Antitumor Activities

Yong Chen[a,b,§], Xiaoyan Wang[a,§], Wei Xiang[a,§], Lin He[a,§], Minghai Tang[a], Fang Wang[a], Taijin Wang[a], Zhuang Yang[a], Yuyao Yi[c], Hairong Wang[a], Ting Niu[c], Li Zheng[a], Lei Lei[a], Xiaobin Li[a], Hang Song[b] and Lijuan Chen[a,*]

[a] State Key Laboratory of Biotherapy/Collaborative Innovation Center of Biotherapy and Cancer Center, West China Hospital of Sichuan University; Chengdu, China.

[b] School of Chemical Engineering, Sichuan University, Chengdu, China.

[c] Department of Hematology and Research Laboratory of Hematology, West China Hospital of Sichuan University, Chengdu, 610041, China.

[§] These authors contributed equally and should be considered as co-first authors

ABSTRACT:

In the present study, a series of novel histone deacetylase (HDAC) inhibitors using the morpholinopurine as the capping group were designed and synthesized. Several compounds demonstrated significantly HDAC inhibitory activities and anti-proliferative effects against diverse human tumor cell lines. Among them, compound **10o** was identified as a potent class I and IIb HDAC inhibitor with good pharmaceutical profile and drug-like properties. Western blot analysis further confirmed that **10o** more effectively increased acetylated histone H3 than panobinostat (LBH-589) and vorinostat (SAHA) at the same concentration in vitro. In *in vivo* efficacy evaluations of HCT116, MV4-11, Ramos and MM1S xenograft models, **10o** showed higher efficacy than SAHA or LBH-589 without causing significant loss of body weight and toxicity. All the results indicated that **10o** could be a suitable candidate for treatment of both solid and hematological cancer.

INTRODUCTION

The histone proteins play important roles in the control of gene expression via modification of chemical reactions such as acetylation, phosphorylation, and methylation.[1, 2] In most cases, histone acetylation enhances transcription while histone deacetylation represses transcription.[3, 4] Inhibition of histone deacetylases (HDACs) causes the accumulation of acetylated histones, bringing about a variety of cell type dependent responses such as apoptosis, differentiation, cell survival, and inhibition of proliferation.[5] There are 18 HDAC isozymes and they are divided into four classes: class I (HDAC 1-3, and 8), class II (HDAC 4, 5, 6, 7, 9, 10) and class IV (HDAC 11)

are all zinc-dependent deacetylases, and class III isozymes including Sirt1 to Sirt7 are NAD^+-dependent isozymes.[6,7] Most HDAC inhibitors fit a three-motif pharmacophoric model consisting of a zinc binding group (ZBG), a linker, and a surface recognition cap region.[8-10] Hydroxamic acid is by far the most common ZBG moiety in HDAC inhibitors owing to its ability to reliably chelate active-site zinc ions.[11, 12] Several HDAC inhibitors such as vorinostat (SAHA)[13, 14], panobinostat (LBH-589)[15], belinostat (PXD-101)[16] were approved by FDA for the treatment of cutaneous T cell lymphoma (CTCL), T cell lymphoma or multiple myeloma. Among them, LBH-589, as a pan-HDAC inhibitor, was approved by FDA for the treatment of multiple myeloma in 2015. A number of HDAC inhibitors are currently at various stages of clinical trials either as single agents or in combination treatment with other chemotherapy drugs for the treatment of solid and hematologic malignancies such as pracinostat (SB939)[17], entinostat (MS275)[18] and rocilinostat (ACY-1215)[19, 20].

The class I phosphatidylinositol 3-kinases (PI3Ks) are also attractive targets for the treatment of cancer.[21-23] The class I PI3Ks are classed into the class IA and class IB including phosphoinositide 3-kinase α (PI3Kα), phosphoinositide 3-kinase β (PI3Kβ), phosphoinositide 3-kinase δ (PI3Kδ), and phosphoinositide 3-kinase δ (PI3Kγ).[24] Several PI3Ks inhibitors are currently in clinical trials for the treatment of cancer such as apitolisib (GDC-0980)[22] and pictilisib (GDC-0941)[25]. However, the efficacy of PI3Ks inhibitors is limited by concurrent activation of other survival- and growth-related pathways. A potential strategy to overcome these limitations is to

combine PI3Ks with other target inhibitors such as MEK inhibitors or HDAC inhibitors to achieve synergistic antitumor activities.[26]

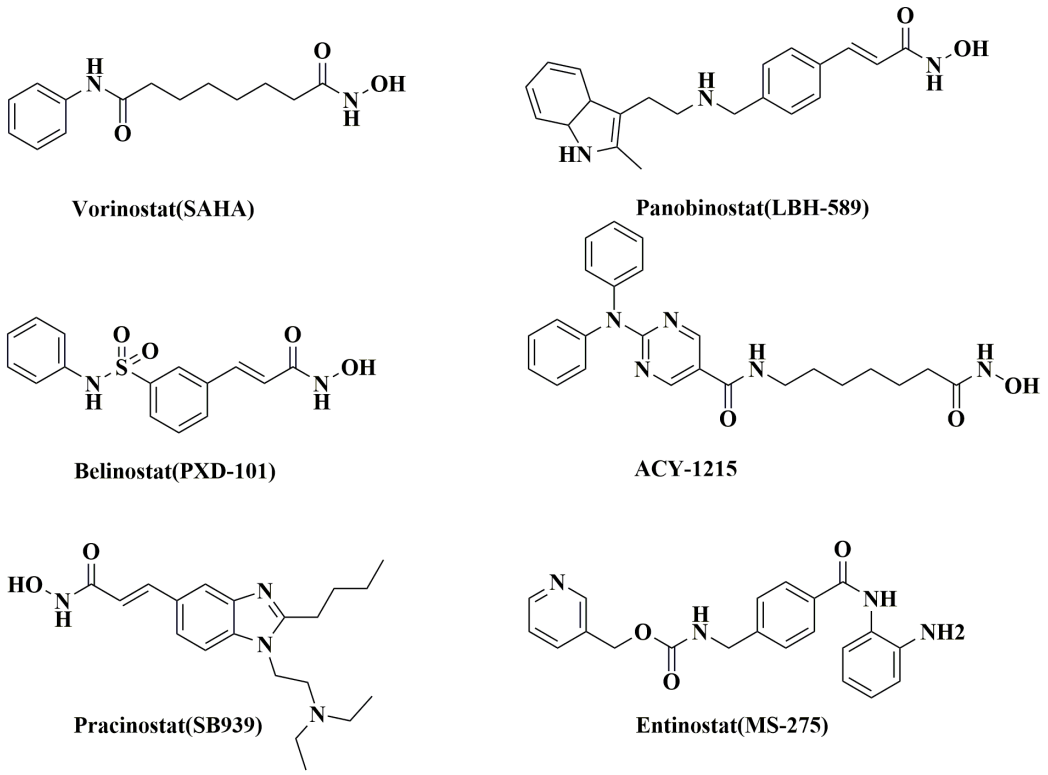

Figure 1. Clinically tested HDAC inhibitors.

In previous reports, Changgeng Qian group successfully achieved CUDC-907 by integrating HDAC inhibitory functionality (hydroxamic acid) into a core structure scaffold (morpholinopyrimidine) shared by several PI3Ks inhibitors.[27-29] CUDC-907 is both a potent pan-inhibitor of HDACs and a PI3Ks inhibitor with IC_{50} values at low nanomolar level. At present, CUDC-907 has been in phase II clinical trials at Curis and was assigned as orphan drug designation in the U.S.A. for the treatment of relapsed or refractory diffuse large B-cell lymphoma (DLBCL) in 2015. CUDC-907 is also in phase I clinical trials for the treatment of breast cancer and multiple myeloma.[30]

Purine as the core scaffold structure has been applied in many drugs of PI3Ks inhibitors, including VS-5584[31], IC-87114[32], and 3-MA[33] (**Figure S1**). Importantly, the morpholine ring is also an important functional group in many PI3Ks inhibitors.[34] Encouraged by the success of Qian group, we thought of designing hybrid pharmacophores to append HDAC recognition cap and hydroxamic acid as a zinc-binding motif (**Figure 2**), in which morpholinopyrimidine was substituted with morpholinopurine scaffold. We designed and synthesized a series of morpholinopurine-based hydroxamic acid derivatives and evaluated their inhibitory activities on the PI3Ks and HDACs. The most potent derivatives were then subjected to in vitro and in vivo antitumor activities. As expected, **10s** and **10t** with pyrimidine at C-2 position of morpholinopurine displayed dual-acting PI3Kα and HDAC1 inhibitory activities. **10s** showed the low IC_{50} values for HDAC1 and PI3Kα with an IC_{50} of 1.04 nM and 1.33 nM in comparison to 1.7 nM and 19 nM of CUDC-907, respectively.[30] Interestingly, when phenyl substituted groups were introduced at C-2 position of morpholinopurine, all these compounds still displayed excellent inhibitory activities for HDAC1 with IC_{50} values ranging from 0.45 nM to 30.10 nM but lost the activities of PI3Ks (IC_{50} > 1000 nM) as single-target inhibitors of HDACs. Among them, **10o** showed better inhibitory activities for class I and class IIb isoforms of HDACs than CUDC-907. Further studies revealed that **10o** showed greater in vitro and in vivo tumor growth inhibition both in hematologic and solid malignancies than LBH-589 and SAHA. Structure-activity relationship (SAR) and computer modeling of these novel compounds were also investigated.

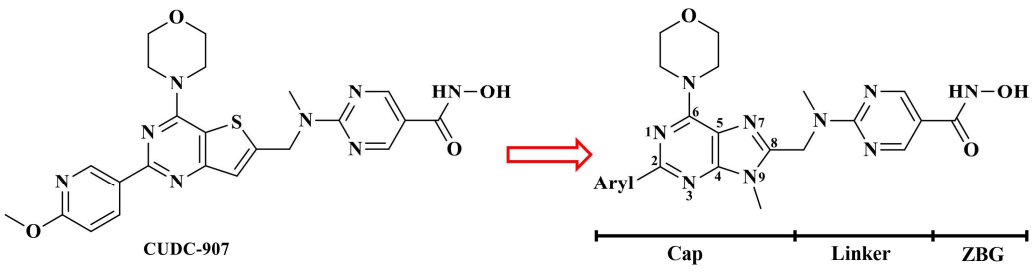

Figure 2. Design of dual-acting HDACs and PI3Ks inhibitors.

CHEMISTRY

The general procedure to synthesize the target molecules **10a−y** has been outlined in **Scheme 1**. Commercially available 2,6-dichloropurine (**1**) as the starting material reacted with morpholine to give **2**, which was treated with CH_3I to obtain **3**. Then the compound **3** was introduced an aldehyde group by reacting with DMF and *n*-BuLi, which got the compound **4**. Then the compound was treated with methylamine methanol solution and $NaBH_4$ in sequence to produce the key intermediate **5**. Treatment of **5** with **6** at room temperature in CH_3CN afforded **7**. The corresponding compounds **9a−y** were obtained by **7** reacting with boronic acid derivatives **8**. Those compounds were directly converted into compounds **10a−y** by NH_2OH.

Scheme 1. Synthesis of the compounds **10a−y**. [a]

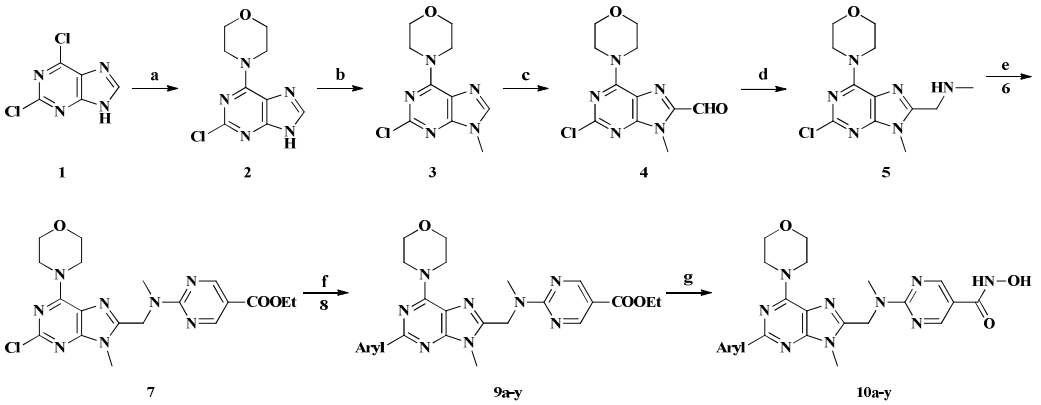

[a] Reagents and conditions: (a) morpholine, CH_3OH, 0 ^oC to rt, 2 h; (b) CH_3I, K_2CO_3, CH_3CN, rt, 3 h; (c) *n*-BuLi, TEMED, DMF, THF, -78 ^oC to -40 ^oC to -78 ^oC, 6 h; (d) Methylamine, rt, 2 h; $NaBH_4$, 0 ^oC, 1 h; (e) 2-chloro-pyrimidine-5-carboxylate, DIPEA, CH_3CN, rt, 5 h; (f) boronic acid derivatives, $PdCl_2(dppf)_2$, $NaHCO_3$, Toluene/EtOH/water (v/v/v, 7/3/2), 80 ^oC, 8 h; (g) NH_2OH, DCM/CH_3OH (v/v, 1/1), rt, 2 h.

In order to study the structure and relationship analysis (SAR) of cap, we also synthesized a series of compounds with *NH*-substitued analogues as the cap (**Scheme 2**). Alternatively, compound **2** was treated with 3,4−dihydropyran to obtain **11** and compounds **15a−l** were prepared according to the same synthetic procedures reported above. The protecting group THP was removed in HCl (con.) methanol solution to give the important intermediates **16a−l**. A series of substituted groups were introduced to *N*−9 position of morpholinopurine to afford **17a−l**. Those compounds were directly converted to hydroxamic acid compounds **18a−l** by NH_2OH.

Scheme 2. Synthesis of the compounds **18a−l**. [a]

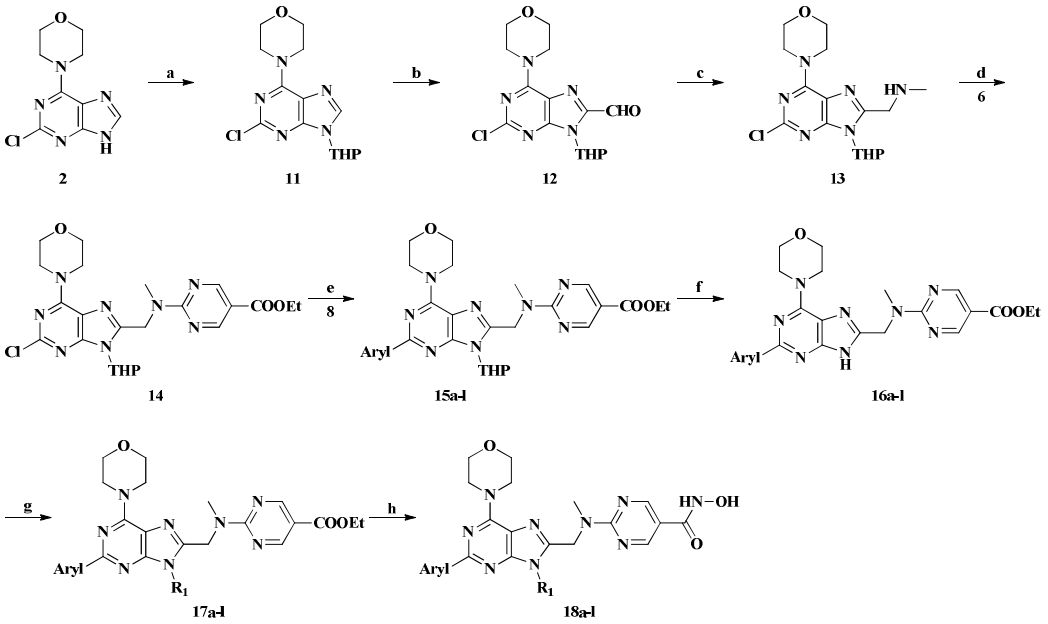

[a] Reagents and conditions: (a) DHP, *p*-TSA, DCM, rt, 2 h; (b) *n*-BuLi, TEMED, DMF, THF, -78 °C to -40 °C to -78 °C, 6 h; (c) Methylamine, rt, 2 h; $NaBH_4$, 0 °C, 1 h; (d) 2-chloro-pyrimidine-5-carboxylate, DIPEA, CH_3CN, rt, 5 h; (e) boronic acid derivatives, $PdCl_2(dppf)_2$, $NaHCO_3$, Toluene/EtOH/ater (v/v/v, 7/3/2), 80 °C, 8 h; (f) HCl, CH_3OH, 50 °C, 2 h; (g) R_1X, Cs_2CO_3, DMF, 80 °C, 4 h; (h) NH_2OH, DCM/CH_3OH (v/v, 1/1), rt, 2 h.

BIOLOGICAL RESULTS AND DISCUSSION

In vitro inhibitory activities of the phenyl substituted analogues. We primarily began our research by screening the inhibitory activities of these compounds on the PI3Kα and HDAC1 isoform. As presented in **Table 1**, phenyl substituted analogues all showed potent HDAC1 inhibition activities but poor PI3Kα inhibitory activities (IC_{50} > 1000 nM). When hydroxyl as an electron-donating group was introduced to meta-position of benzene, **10b** reached an IC_{50} as low as 0.55 nM against HDAC1. Similarly, **10c** showed equivalent potency with **10b** with an IC_{50} of

0.45 nM when methoxyl group was introduced to para-position of benzene. In contrast, **10f** decreased HDAC1 inhibition activity with an IC_{50} of 5.10 nM when trifluoromethyl as an electron-withdrawing group was introduced to para-position of phenyl. These results suggest that electron-donating groups improve HDAC1 inhibition activity and electron-withdrawing groups decrease HDAC1 inhibition activity. As expected, **10e**, **10g**, **10h** and **10j** all displayed decreased inhibition activities toward HDAC1 according to the similar rule. When *N-H* of the aniline was substituted by methyl, ethyl, and isopentene group separately, **10p**, **10q** and **10r** showed significant decrease in inhibitory activities with the extension of chain length of substituent groups.

To investigate the effects of chain length on HDAC1 inhibitory activity, **10k−n** were synthesized. Dramatically, the activity gradually decreased with the increase of chain length from methyl to *t*-butyl and IC_{50} ranging from 1.00 nM to 10 nM. Interestingly, most compounds such as **10a−e**, **10h−k** and **10o−q** all showed better inhibitory activity of HDAC1 isoform than CUDC-907, suggesting that morpholinopurine as a substituted core structure scaffold showed better HDAC1 activity than morpholinopyrimidine.

Table 1. IC_{50} values for enzymatic inhibition of HDAC1 and PI3Kα.

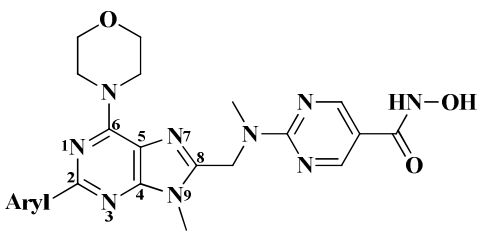

Compd	Aryl	IC_{50}[a] (nM)		Compd	Aryl	IC_{50}[a] (nM)	
		HDAC1	PI3Kα			HDAC1	PI3Kα
10a	Cl	1.10	>10000	**10k**	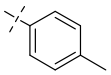	1.00	>10000
10b	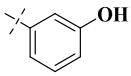	0.55	>10000	**10l**	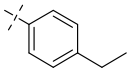	1.98	>10000
10c	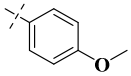	0.45	>10000	**10m**	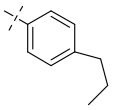	6.15	>10000
10d	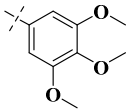	1.02	>10000	**10n**	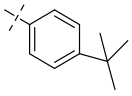	10.01	>10000
10e	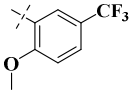	1.59	>10000	**10o**	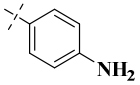	0.65	>1000
10f	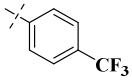	5.10	>10000	**10p**	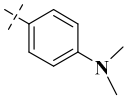	0.81	>10000
10g	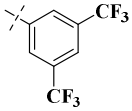	30.10	>10000	**10q**	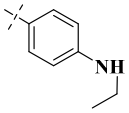	1.10	>10000
10h	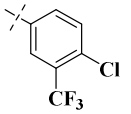	1.01	>10000	**10r**	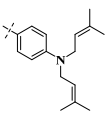	10.00	>10000
10i	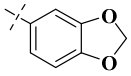	0.97	>1000	**SAHA**		11	>10000
10j	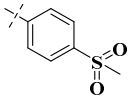	0.85	>1000	**CUDC-907**		1.7	19

[a] IC_{50} values for enzymatic inhibition of HDAC1 and PI3Kα. The IC_{50} values are the means of at least two experiments, with intra- and inter-assay variations of < 10%.

In vitro inhibition activities of six-membered *N*-containing heterocyclic analogues. When six-membered *N*-containing heterocyclic was introduced to instead of phenyl at C-2 position of morpholinopurine, we synthesized compounds **10s−y**.

The enzyme inhibitory activities on HDAC1 and PI3Kα were evaluated (**Table 2)**. **10s−y** all showed excellent inhibitory activity toward HDAC1 with nanomolar IC_{50} values, but inhibitory activity for PI3Kα differed obviously. **10s** and **10t** exhibited potent inhibitory activity both on HDAC1 and PI3Kα when pyrimidine was introduced to the C-2 position of morpholinopurine. **10s** with amino group at para-position of the pyrimidine displayed stronger inhibitory activities on HDAC1 and PI3Kα with respective IC_{50} values of 1.04 nM and 1.33 nM in comparison to 1.7 nM and 19 nM of CUDC-907. **10t** without amino group displayed slightly lower activity on PI3Kα with an IC_{50} of 28.06 nM. In contrast, pyridine-based analogues **10u−y** dramatically decreased PI3Kα inhibition activity above micromolar level. These results suggested that aminopyrimidine plays an important role to maintain the dual-target inhibitory activities on HDAC1 and PI3Kα.

Table 2. IC_{50} values for enzymatic inhibition of HDAC1 and PI3Kα.

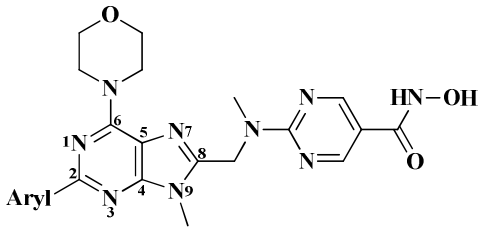

Compd	Aryl	IC_{50}[a] (nM)	
		HDAC1	PI3Kα
10s	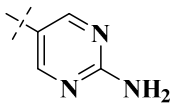	1.04	1.33
10t	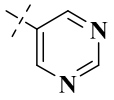	1.14	28.06
10u	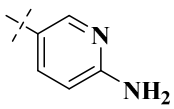	1.11	>1000

10v	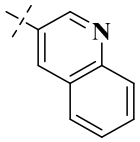	1.60	>1000
10w	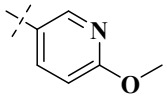	1.00	>1000
10x	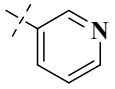	0.49	>1000
10y	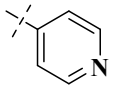	0.55	>1000
SAHA		11	>10000
CUDC-907		1.7	19

[a] IC_{50} values for enzymatic inhibition of HDAC1 and PI3Kα. The IC_{50} values are the means of at least two experiments, with intra- and inter-assay variations of < 10%.

In vitro inhibition activities of *N-H* substituted analogues. To understand the structure-activity relationship of *N-H* substituted analogues, we synthesized **18a−l** to probe the effects of different substitutions on inhibitory potency of HDAC1 and PI3Kα. As shown in **Table 3,** when R_1 changed from methyl to ethyl, the potency on HDAC1 was retained. However, when R_1 changed from ethyl to isopropyl and cyclopentyl, the potency on HDAC1 decreased significantly, the inhibitory activity of **18a** on HDAC1 was 100-fold over **18b** and **18c**. The similar results were also observed in **18d−f**, **18g−i**, and **18j−l**. These results indicated that methyl was crucial to contribute to improving the inhibition activities on HDAC1 and PI3Kα. However, all these compounds did not improve the potency on PI3Kα in comparison with **10s**.

Table 3. In vitro HDAC1 and PI3Kα inhibitory activities.

188

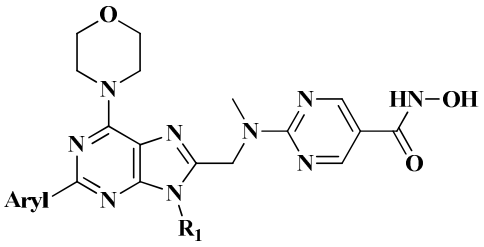

Compd	Aryl	R_1	IC_{50}[a] (nM)		Compd	Aryl	R_1	IC_{50}[a] (nM)	
			HDAC1	PI3Kα				HDAC1	PI3Kα
10c		Me	0.45	>1000	**10s**		Me	1.04	1.33
18a	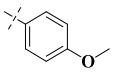		1.00	>1000	**18g**	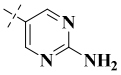		2.62	28.42
18b			110	>1000	**18h**			240	>1000
18c			125	>1000	**18i**			300	>1000
10o		Me	0.65	>1000	**10w**		Me	1.00	>1000
18d	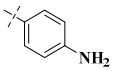		1.37	>1000	**18j**	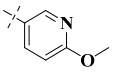		1.60	>1000
18e			165	>1000	**18k**			62	>1000
18f			190	>1000	**18l**			67	>1000
SAHA			11	>10000	**CUDC-907**			1.7	19

[a] IC_{50} values for enzymatic inhibition of HDAC1 and PI3Kα. The IC_{50} values are the means of at least two experiments, with intra- and inter-assay variations of < 10%.

In vitro cell growth inhibitory effects in MV4-11, A2780s, and HCT116 cells.

After the synthesis and evaluation for enzymatic activity assays of these compounds, anti-proliferative effects of these compounds against MV4-11 cells, A2780s cells, and HCT116 cells were tested using MTT assay. SAHA, LBH-589, and CUDC-907 were used as references (**Table 4**). A total of 29 compounds showed strong

anti-proliferative activity with most IC_{50} values less than 100 nM. Among them, **10o**, **10p, 10q**, **10w** and **10y** showed comparable inhibitory activities to CUDC-907 and LBH-589, but much stronger than SAHA against all three types of cancer cells. Although **10s** was the same as CUDC-907 to be a dual-target inhibitor, its inhibitory activity on tumor cells was inferior to CUDC-907.

For the series of compounds **10a−y**, compounds with aromatic rings substituted at the C-2 position of the purine ring (**10b−y**) were generally more potent inhibitors than the chlorine substituted (**10a**). Proper substitution of C-4 position amino of **10o**, such as double methyl (**10p**) and single ethyl (**10q**), caused a little decrease of the anti-proliferative activities than the non-substituted (**10o**); while double dimethylallyl substituted analogue of amino (**10r**) resulted in a sharp decrease in potency over **10o**. As the substitution group length at C-4 position of benzene increased, from methyl to *t*-butyl (**10k−n**), the compounds suffered a sharp decrease in anti-proliferative activity. In corporation of trifluoromethyl group of phenyl ring (**10f−h**), the anti-proliferative activities decreased.

Table 4. Cell growth inhibitory effects for all compounds, SAHA, LBH-589 and CUDC-907.

Compd	**IC_{50} ± SEM[a] (nM)**		
	MV4-11	**A2780s**	**HCT116**
10a	37.39±6.32	85.73±12.16	66.55±2.86
10b	7.65±1.08	13.65±0.49	13.02±1.32
10c	4.80±1.43	31.81±3.08	14.84±5.47

10d	0.95±0.07	39.31±3.56	15.38±1.58
10e	2.69±0.62	224±12	54.35±5.18
10f	3.67±0.32	45.78±1.58	10.63±1.12
10g	65.04±4.45	560±16	89.32±5.16
10h	148±12	300±6	381±25
10i	4.09±0.71	18.48±0.10	9.25±1.08
10j	1.04±0.09	12.53±1.58	7.85±2.10
10k	3.32±2.94	11.30±1.29	5.77±1.20
10l	30.80±3.20	3.74±0.59	7.05±0.32
10m	35.30±3.20	52.06±8.37	57.63±6.52
10n	160±12	286±25	160±16
10o	0.15±0.02	6.98±1.82	0.74±0.10
10p	0.89±0.10	2.36±0.89	4.73±1.07
10q	2.51±0.50	9.17±3.56	10.26±1.27
10r	44.77±13.27	127.10±12.40	76.46±9.83
10s	7.65±0.79	117.60±3.42	214.20±16.35
10t	59.8±3.20	75.08±4.93	46.66±3.20
10u	4.00±0.41	181±22	40.24±7.04
10v	7.46±0.72	129.50±8.15	9.22±0.34
10w	0.69±0.05	12.94±1.34	16.13±2.30
10x	1.15±0.28	51.69±0.51	13.99±2.35
10y	0.19±0.05	90.63±1.53	1.99±0.30
18a	78.82±12.16	107.60±24.73	241.10±25.72
18d	4.85±0.87	30.27±0.18	27.65±2.39

18g	14.63±1.42	240±15	317±20
18j	8.85±0.87	37.28±0.18	17.95±2.09
SAHA	230±24.2	870±68.4	1450±259.7
CUDC-907	0.43±0.09	6.15±1.02	7.34±1.98
LBH-589	2.97±0.11	8.32±2.33	3.36±0.36

[a] IC_{50} = compound concentration required to inhibit tumor cell proliferation by 50%; data are expressed as the mean ± SEM from the dose-response curves of at least three independent experiments.

In vitro inhibition of the enzymatic activities of HDACs and PI3Ks. In our progress of research, we found that although **10b**, **10c**, **10d**, **10i−k**, **10o−q**, **10v**, and **10w−y** all showed excellent HDAC inhibitory effects and anti-proliferative activities on tumor cells, most of these compounds had poor solubility in several solvents even dimethyl sulfoxide. Their disadvantages limited further dose administration in vivo evaluation. Considering the solubility and suitable administration as properties required for therapeutic application, we chose **10c**, **10o**, **10w**, **10s**, and **10y** to ascertain the potency of selected compounds across the broader family of HDACs and PI3Ks isoforms, CUDC-907 and LBH-589 were also chosen as positive controls. The data were shown in **Tables 5** and **6**. As described previously, **10s** displayed the most potent inhibition activities toward PI3Ks, as well as high potency toward HDACs as a dual-acting inhibitor. **10c**, **10o**, **10w** and **10y** all displayed remarkable inhibitory activities toward class I (HDACs 1-3, 8) and class IIb (HDACs 6, 10) isoforms of HDACs. In comparison to LBH-589 and CUDC-907, most of these compounds showed better isoforms selectivity for class I and class IIb isoforms over class IIa

(HDACs 4, 5, 7, 9), suggesting that **10c**, **10o**, **10w** and **10y** are all class I and class IIb isoform inhibitors. Among them, only **10s** was identified as a dual-acting inhibitor toward PI3Ks and HDACs.

Table 5. The enzymatic activities for HDACs of the selected compounds.

Classes of HDACs	isoforms	IC_{50} [a] (nM)						
		10c	**10o**	**10w**	**10s**	**10y**	**CUDC-907**	**LBH-589**
class I	HDAC1	0.45	0.65	1.00	1.04	0.55	1.7	1.26
	HDAC2	3.90	2.90	11.46	2.62	2.80	5.0	3.28
	HDAC3	2.55	3.40	4.65	3.29	2.70	1.8	2.27
	HDAC8	92.92	24	217	22	11	191	4.86
class IIa	HDAC4	>1000	>1000	>1000	653	>1000	409	337.8
	HDAC5	>1000	750	>1000	484	>1000	674	190.3
	HDAC7	>1000	>1000	>1000	650	895	426	4354
	HDAC9	>1000	>1000	>1000	>1000	>1000	554	887.8
class IIb	HDAC6	7.78	6.40	18.22	22	2.70	27	4.16
	HDAC10	6.85	2.80	17.55	2.83	0.86	2.8	4.45
class IV	HDAC11	>10000	>1000	>1000	>1000	835	5.4	4112

[a] IC_{50} values for enzymatic inhibition of HDACs. The IC_{50} values are the means of at least two experiments, with intra- and inter assay variations of < 10%.

Table 6. The enzymatic activities for class I PI3Ks of the selected compounds.

Class I	IC_{50} [a] (nM)						
	10c	**10o**	**10w**	**10s**	**10y**	**CUDC-907**	**LBH-589**

PI3Kα	>10000	>1000	>1000	1.33	>1000	19	>10000
PI3Kβ	>10000	>10000	>1000	34	>10000	54	>10000
PI3Kγ	>10000	>10000	255	8.10	>10000	311	>10000
PI3Kδ	>10000	>10000	493	15	>10000	39	>10000

[a] IC_{50} values for enzymatic inhibition of PI3Ks. The IC_{50} values are the means of at least two experiments, with intra- and inter assay variations of <10%.

In order to investigate whether the HDAC1 IC_{50} value of selected compounds is likely close to its actual IC_{50}, we performed a HDAC enzyme activity assay utilizing nuclear extracts from the cell line of HeLa. As shown in **Table 7**, **10c**, **10o**, **10s**, **10w**, and **10y** showed the similar inhibition to HDACs to CUDC-907 but superior to SAHA, the IC_{50} values of **10c**, **10o**, **10s**, **10w**, and **10y** on HDAC were 3.4, 3.2, 3.3, 6.1, 6.3 nM, respectively. LBH-589 exhibited the most inhibition on HDACs among these compounds.

Tubulin acetylation and histone H3 acetylation induction of selected compounds. Cytoblot experiments were performed to further evaluate the histone H3 acetylation (Ac-H3) and tubulin acetylation (Ac-Tub) of selected compounds. As exhibited in **Table 7**, **10s** showed comparable Ac-H3 and Ac-Tub induction in cellular assays to CUDC-907, which were in line with the in vitro enzymatic data. **10c**, **10o**, **10w** and **10y** all showed the similar activities to LBH-589 but better activities than SAHA in tubulin acetylation and histone H3 acetylation induction.

Table 7. Tubulin acetylation and histone H3 acetylation induction and against HeLa cells of selected compounds, LBH-589, CUDC-907, and SAHA.

Compd	IC_{50} [a] (nM)	EC_{50} [b] (nM)	
	HeLa	Ac-Tub	Ac-H3
10c	3.40±0.1	248.35±152.52	98.58±13.60
10o	3.20±0.1	211.05±37.69	112.96±46.58
10s	3.30±0.8	143.7±46.53	123.2±22.77
10w	6.10±1.0	198.6±17.11	117.65±5.44
10y	6.30±2.3	187.9±10.89	142.01±105.92
LBH-589	0.83±0.1	150.71±111.01	169.5±4.67
CUDC-907	6.80±0.4	221.75±52.40	126.25±4.03
SAHA	11.5±0.7	399.25±34.29	377.48±23.16

[a] IC_{50} values of HeLa Nuclear Extract HDAC inhibition. [b] EC_{50} values of tubulin acetylation and Ac-H3 are based on cytoblot experiments run in duplicate in A2780s cells. Data are expressed as the mean ± SEM from the dose−response curves of at least three independent experiments.

In order to confirm whether compound **10s** is a dual-acting selective inhibitor toward PI3Ks and HDACs and **10c**, **10o**, **10w** and **10y** are all class I and class IIb isoform inhibitors, we selected two compounds **10s** and **10o** to examine the protein kinases inhibitory profile against 100 selected recombinant human protein kinases. As shown in **Tables 6** and **7**, compound **10s** exhibited excellent inhibitory activities for HDACs and PI3Ks, the IC_{50} values of **10s** on HDAC1, PI3Kα, PI3Kβ, PI3Kγ and PI3Kδ were 1.04, 1.33, 34, 8.10 and 15 nM, respectively. In contrast, the IC_{50} values of CUDC-907 on HDAC1, PI3Kα, PI3Kβ, PI3Kγ and PI3Kδ were 1.7, 19, 54, 311 and 39 nM, respectively. **10s** showed weak inhibitory activity against cKit, cSRC (h)

and Src (T341M) (the binding affinities were 38, 56 and 39 at 1 μM). However, compound **10s** showed almost no inhibitory activity against the other selected protein kinases (**Table S1)**. These data demonstrates that **10s** is a dual-acting selective inhibitor toward PI3Ks and HDACs. Compound **10o** only showed strong inhibitory activity against HDACs but had no inhibitory activity against the 100 selected recombinant human protein kinases, demonstrating that compound **10o** is a single-target class I and class IIb HDAC inhibitor.

To further confirm the selectivity of **10s** and **10o** on PI3Ks and HDACs, The effects of **10s** and **10o** on the activities of mTOR, PI3K and Akt in HCT116 cells treated with indicated concentrations for 6 h were investigated by western blot analysis (**Figure S2**). **10s** reduced the levels of mTOR, PI3K and Akt phosphorylations in a concentration dependent manner. However, the levels of phosphorylation of mTOR, PI3K and Akt were not obviously altered by **10o**. The data further demonstrates that **10s** is a dual-acting selectivity inhibitor toward PI3Ks and HDACs and **10o** is a single-target class I and class IIb HDAC inhibitor.

Molecular Docking Study. To better understand the different activities of **10s** and **10o** on PI3Kα, the molecular docking was performed (**Figure 3A** and **Figure S3)**. From the docking results, we found that the oxygen of the morpholine group of **10s** forms a hydrogen bond interaction with the backbone *NH* group of Val-851 in the hinge region, the morpholine ring has the hydrophobic contacts with the residues of Val-851, Met-922, Ile-932, and the purine core forms hydrophobic interactions with the side chains of Met-772 and Ile-932. These interactions are considered as critical

forces which determine the binding capacity of PI3Kα inhibitors. And the tail of hydroxamic acid could interact with Ser-854 on the entrance of the ATP pocket. The pyrimidine ring linked with hydroxamic acid could interact with the indole ring of Trp-780 by means of π-π stacking. More importantly, the amino group on the pyridine ring of **10s** forms two hydrogen bonds to the residues of Asp-810 and Asp-933, while the pyrimidine nitrogen atoms form additional hydrogen interactions with the phenolic hydroxyl of Tyr-836 and the catalytic lysine Lys-802. In contrast, due to the replacement of pyrimidine ring, the aniline of **10o** could not form additional hydrogen interactions with the residues of Tyr-836 and Lys-802. And, with the stronger hydrogen bonding capabilities, compound **10s** may have higher inhibitory activity against PI3Kα than compound **10o**. In according with the enzymatic inhibition level described previously, **10s** could inhibit PI3Kα efficiently with IC_{50} value of 1.33 nM, but **10o** showed weak inhibitory activity on PI3Kα (IC_{50} > 1000 nM).

The molecular docking with compound **10s** and **10o** in HDAC1 was also performed (**Figure 3B** and **Figure S4**). The catalytic Zn^{2+} is coordinated by the hydroxamic acid, Asp-264, Asp-176 and His-178. Also, the hydroxamic acid tail forms hydrogen interaction with the residues of His-140 and Tyr-303. In the cap region, the purine ring forms a π-π stacking interaction with residues of Phe-150 and Phe-205. And the nitrogen atoms, linking the pyrimidine ring in **10s** and benzene ring in **10o**, form hydrogen interaction with Gln-26, respectively.

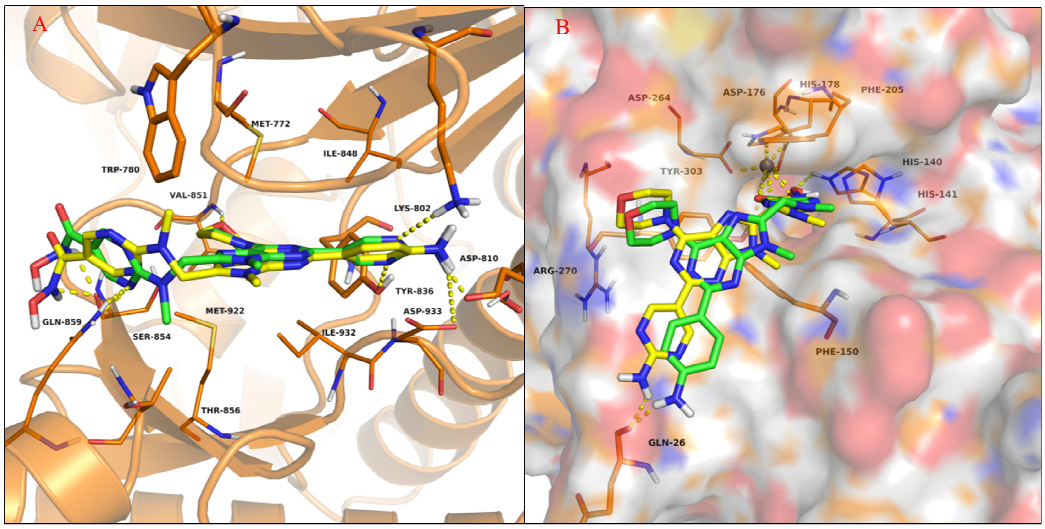

Figure 3. (A) Proposed binding mode of compound **10s** (green stick) and **10o** (yellow stick) within the ATP pocket of PI3Kα (PDB code 4L23). And the dash lines represent the H-bond interaction between compound **10s** and PI3Kα. (B) Representation of the predicted binding modes of **10s** (yellow stick) and **10o** (green stick) in the active site of HDAC1 (PDB code 4BKX), yellow dash lines indicate the H-bond interaction between **10o** and HDAC1. For clarity, oxygen and nitrogen atoms are shown in red and blue respectively.

Anti-tumor activity in vivo. Since **10s**, **10c**, **10o**, **10w** and **10y** all exhibited good in vitro anti-proliferative activities, we primarily established a MV4-11 xenograft NOD/SCID mouse model to investigate the effects of **10c**, **10s**, **10w**, **10y**, and **10o** on tumor growth, with SAHA administrated for comparison. The administration, dosing schedules, and results are presented in **Table 8**.

Table 8. Summary of tumor growth inhibition of selected compounds.

Tumor	compd	administration			statistical significance[b]	max body weight loss(%)(day)	survivors (day)	tumor mass change(%)
		schedule[a]	dose (mg/kg)	route				

	10c	Q2D×11	10	iv	***	8.1(7)	4/6	65.3
	10s	Q2D×11	10	iv	**	6.4(13)	4/6	45.1
MV4-11	**10w**	Q2D×11	10	iv	***	14.9(11)	5/6	63.4
	10y	Q2D×11	10	iv	***	2.1(19)	5/6	64.3
	10o	Q2D×11	10	iv	***	3.6(19)	6/6	65.6
	SAHA	Q2D×11	50	ip	ns	3.0(17)	6/6	0
	10o	Q2D×8	2.5	iv	***	3.9(4)	6/6	49.4
HCT116	**10o**	Q2D×8	5	iv	***	2.1(12)	6/6	53.3
	10o	Q2D×8	10	iv	***	1.4(10)	6/6	68.2
	SAHA	Q2D×8	50	ip	**	5.2(8)	6/6	32.4
Ramos	**10o**	Q2D×6	10	iv	***	0.8(12)	8/8	83.9
	LBH-589	Q2D×6	10	ip	***	1.9(7)	5/8	16.6
	10o	Q2D×6	2.5	iv	***	2.4(12)	7/7	45.1
MM1S	**10o**	Q2D×6	5	iv	***	3.1(9)	7/7	69.2
	10o	Q2D×6	10	iv	***	2.1(12)	7/7	75.1
	LBH-589	Q2D×6	10	ip	***	5.1(12)	7/7	49.2

[a] Q2D, every 2 days. [b] One-way ANOVA followed by Dunnett's multiple comparison test was used to determine the statistical significance of tumor volume between a treatment group and the control (vehicle) group: ns=not significant, (**) $p<0.01$, and (***) $p<0.001$.[5]

As displayed in **Table 8**, 1**0c**, **10w**, **10y**, and **10o** all exhibited antitumor activities. The tumor growth on MV4-11 was significantly suppressed by 65.3, 63.4, 64.3 and 65.6% (tumor growth inhibitory rate [TGI], as indicated the percentage of tumor mass change values) after intravenous administration of 1**0c**, **10w**, **10y**, and **10o**

at 10 mg/kg, respectively. In contrast, SAHA had no inhibitory activity at 50 mg/kg ip administration on the MV4-11 xenograft model. **10s** showed the worst inhibitory effect with the TGI of 45.1% which is in consistent with in vitro potency. In addition, **10c** and **10s** exhibited some toxicity and two of mice died during the treatment period. At the same dose, **10w** and **10y** both retained potent inhibition on MV4-11 but both still caused one mouse death. **10o** could inhibit tumor growth with TGI of 65.6%. Among the five compounds, **10o** exhibited the most potent antitumor activity without significant toxicity: slight body weight change and no death of mice were observed during the treatment period. Furthermore, **10o** showed the best water-solubility among the five compounds. Hence, **10o** was selected for further in vitro and in vivo antitumor evaluation in solid tumor and hematological models.

We then established HCT116 xenograft model since this model had been successfully used for HDAC inhibitors evaluation such as dacinostat[35] and belinostat[36]. As displayed in **Table 8** and **Figure 4A**, iv administration of **10o** dose-dependently inhibited tumor growth, the significant antitumor activity was observed at dose as low as 2.5 mg/kg (TGI = 49.4%, $p<0.001$), 5 and 10 mg/kg of **10o** caused respective TGI of 53.3% and 68.2%. In contrast, SAHA only showed 32.4% of TGI at 50 mg/kg ip administration. In addition, **10o** did not cause significant weight loss in HCT116 xenograft model during the treatment period.

In vitro and in vivo anti-proliferative activities of 10o in hematological tumor cells.

As most HDAC inhibitors are used for hematological cancer treatment, **10o** was further investigated the anti-proliferative activities against 8 kinds of hematological tumors including multiple myeloma (U266, RPMI-8226 and MM1S cells) and B cell lymphoma (OCI-LY1, HBL-1, Ramos, Raji and SUDHL4 cells) by MTT, and

LBH-589 was chosen as a positive control (**Table S2**). **10o** showed better or comparable anti-proliferative potential to LBH-589, and the IC_{50} values were ranging from 0.78 to 12.85 nM in these tumor cell lines.

It was recently announced that LBH-589 had been approved by FDA for the treatment of multiple myeloma as a new HDAC pan-inhibitor. LBH-589 has also been licensed or at various stages of clinical evaluation for the treatment of B cell lymphoma. We further established a multiple myeloma MM1S and a B cell lymphoma Ramos NOD/SCID xenograft models to validate the antitumor effect of **10o** (**Table 8**，**Figure 4B** and **4C**). In MM1S tumor model, **10o** dose-dependently inhibited tumor growth, low-dose administration of **10o** (2.5 mg/kg iv) could effectively inhibit tumor growth and the TGI was 45.1%, which was comparable to LBH-589 at 10 mg/kg ip treatment (TGI, 49.2%). However, **10o** at 5 mg/kg iv treatment showed much more efficacious in inhibiting tumor growth than LBH-589 and the TGI was up to 69.2%. Further increased dose of 10 mg/kg of **10o** caused the TGI to 75.1%. In addition, there is no significant weight loss of NOD/SCID mice during the treatment period. Surprisingly, in B cell lymphoma Ramos NOD/SCID xenograft model, **10o** at 10 mg/kg iv treatment caused significantly tumor growth inhibition, the TGI was 83.89%. In contrast, LBH-589 was not sensitive to this model and had no activity (TGI, 16.6%), and three of eight mice died during experimental period. These results confirmed that **10o** showed superior antitumor to LBH-589 and could be used as a novel HDAC inhibitor to be further researched on the therapy of both hematological tumors and solid tumors.

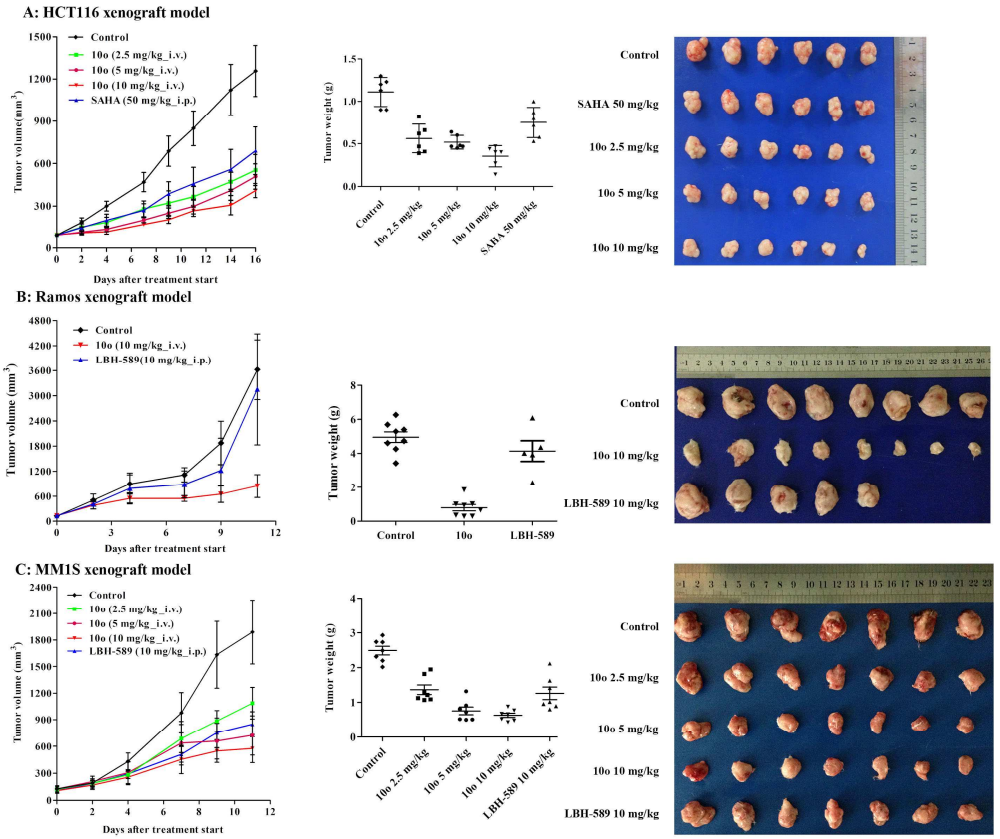

Figure 4. Antitumor activities of **10o**, SAHA and LBH-589 on the xenograft models. (A) Antitumor growth of **10o** on the HCT116 xenograft model. (B) Antitumor growth of **10o** on Ramos xenograft model. (C) Antitumor growth of **10o** on MM1S xenograft model. **10o** was dissolved in physiological saline containing 20% captisol with the pH adjusted to 6). SAHA (50 mg/kg) was dissolved in physiological saline containing 5% DMSO and 30% PEG400. LBH-589 was dissolved in physiological saline containing 2% DMSO, 2% Tween 80 and 15% PEG400.

Formation of salts is a well-known technique to modify and optimize the solubility to improve the pharmacokinetics and increase the bioavailability. As depicted in **Table S3**, the oral bioavailability of **10o** was 4.83%, which is comparable to LBH-589 (4.62%, Female Balb/c nude mice).[37] However, the oral bioavailability of

10o·CH_3SO_3H in SD rats was increased to 14.21%, much higher than LBH-589. Encouragingly, the oral bioavailability of **10o·CH_3SO_3H** in beagle dogs was up to 41.82%. The low clearance, rapid elimination half-life and good bioavailability indicated that **10o** may be suitable both for oral and intravenous dosing for further development as an anticancer agent.

Upregulation effects of histone H3 and α-tubulin. We attempted to validate the observed biochemical potencies of the **10o** in a cellular context by examining its HDACs activity in comparison with SAHA and LBH-589. The effects of **10o** on the acetylation level of histone H3 (a known substrate for HDACs 1-3) and α-tubulin (a known substrate for HDAC6), the biomarkers of HDAC inhibition[38], in MV4-11 and HCT116 cells treated with different concentrations are shown in **Figure 5**. As expected, in agreement with the relative potency in class I (HDAC 1-3, 8) inhibition, **10o** induced a concentration-dependent increase of the acetylated histone H3 from 0.02 μM to 2 μM, which is comparable to LBH-589, however, SAHA only slightly upregulated the acetylated histone H3 at concentration of 2 μM. Furthermore, both **10o** and LBH-589 upregulated acetylated α-tubulin in a concentration-dependent manner, but SAHA induced acetylated α-tubulin increase at slightly higher concentration. These results showed that **10o** was a class I and class IIb isforms HDAC inhibitor.

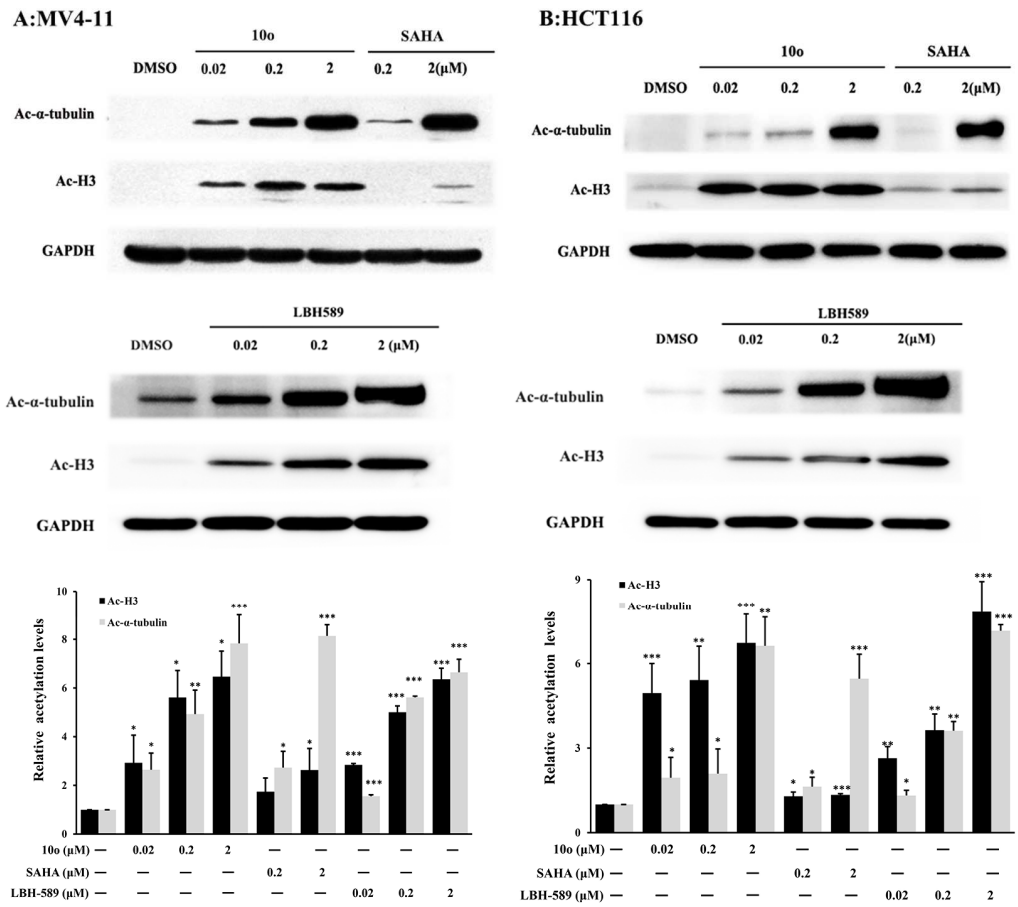

411

412 **Figure 5.** Western blot analysis of acetylated α-tubulin, acetylated histone H3 in
413 MV4-11 and HCT116 cell lines after 6 h treatment with compounds **10o**, LBH-589 at
414 0.02, 0.2, 2 μM and SAHA at 0.2, 2 μM. GAPDH was used as a loading control.

415 **CONCLUSIONS**

416 We chose morpholinopurine as a core structure scaffold of cap group, and a
417 series of hydroxamic acid analogues were prepared and evaluated for bioactivity in
418 vitro and in vivo. The inhibitory activities on the HDAC1 and PI3Kα isoforms of the
419 synthesized compounds and a SAR analysis revealed that the strategy successfully
420 achieved the target to find novel and highly efficient small molecule inhibitors of
421 HDACs. The most potent dual-target inhibitor **10s** displayed efficient activities for

PI3Kα with an IC_{50} of 1.33 nM, as well as a potent pan-HDAC inhibitor. Because of toxicity and poor water-solubility, **10s** could be further optimized to improve water-solubility and reduce toxicity. Compound **10o** showed better activities for class I and class IIb isoforms over other isoforms of HDACs. Subsequently, the western blot analytical results further confirmed that **10o** displayed excellent potency toward HDACs. **10o** displayed anti-proliferative activity with IC_{50} values of 0.15-12.85 nM against diverse cancer cell lines including non-solid and solid tumor cells. Most importantly, **10o** showed substantial antitumor activity with tumor growth inhibition of 65.6% and 68.2% in MV4-11 and HCT116 xenograft models after iv treatment with 10 mg/kg, respectively, which was greater than SAHA groups (0 and 32.4% respectively to MV4-11 and HCT116 xenograft models, 50 mg/kg, ip). In MM1S xenograft model, **10o** inhibited tumor growth up to 75.1%, much stronger than LBH-589 (49.2%) at the same dose. Surprisingly, **10o** showed much higher antitumor activity in B cell lymphoma Ramos model, further underlying mechanism should be investigated in near future. Moreover, **10o·CH_3SO_3H** has a better oral bioavailability of 14.21% in SD rats than LBH-589 (4.62%), and excellent bioavailability in beagle dogs (41.82%), suggesting that **10o** is suitable both for oral and intravenous dosing for treating cancers. In future work, the antitumor properties of **10o·CH_3SO_3H** via oral administration would be evaluated. By far, the existing data indicated that **10o** is a potential promising histone deacetylase inhibitor for the therapy of both hematological tumors and solid tumors.

Experimental Section

Chemistry. All the chemical solvents and reagents, which were analytically pure without further purification, were commercially available. TLC was performed on 0.20 mm Silica Gel 60 F_{254} plates (Qingdao Haiyang Chemical, China).^{1}H NMR and ^{13}C NMR spectra were recorded on a BrukerAvance400 spectrometer (Bruker Company, Germany) or Varian spectrometer (Varian, Palo Alto, CA), using TMS as an internal standard. Chemical shifts were given in ppm (parts per million). Mass spectra were recorded on Q-TOF Priemier mass spectrometer (Micromass, Manchester, UK). The purity of each compound (>95%) was determined on an Waters e2695 series LC system (column, Xtimate C18, 4.6 mm ×150 mm, 5 μm; mobile phase, methanol (60%)/H_2O (40%); low rate, 1.0 mL/min; UV wavelength, 254-400 nM; temperature, 25 ^{o}C; injection volume, 10 μL).

General Procedures of Method A for the Synthesis of 10a−y.

4-(2-chloro-9*H*-purin-6-yl)morpholine (**2**). To the mixture of **1** (18.9 g, 100 mmol, 1 equiv) in methanol (500 ml) was added morpholine (13 ml, 150 mmol, 1.5 equiv) slowly under ice-bath. The mixture was stirred for 10 minutes, and stirred at room temperature for another 2 hours. Upon the reaction completed, large amounts of precipitates formed. The precipitates were collected by filtration and the filtrate was removed under reduced pressure to get the solid. The solid was dissolved in CH_2Cl_2, washed by diluted HCl solution, water and saturated brine three times. The combined organic layers were dried over Na_2SO_4, filtered and the solvent was removed under reduced pressure. The combined solids were crude product without purification. Yield

95%, white power solid. ^{1}H NMR (400 MHz, DMSO-d_6) δ: 3.72 (t, 4H, J = 4.8 Hz), 4.18 (m, 4H), 8.15 (s, 1H), 13.21 (s, 1H). MS (ESI), m/z: 240.2 $[M+H]^+$.

4-(2-chloro-9-methyl-9*H*-purin-6-yl)morpholine (**3**). To the mixture of **2** (23.9 g, 100 mmol, 1 equiv) in acetonitrile (500 ml) was added Cs_2CO_3 (48.75 g, 150 mmol, 1.5 equiv), followed by CH_3I (9.4 ml, 150 mmol, 1.5 equiv) slowly. The mixture was stirred at room temperature for 4 hours. The mixture was filtrated to get filtrate A and residue. The residue was washed by CH_2Cl_2 three times to get filtrate B. The combined filtrates were concentrated under reduced pressure to get solid. The solid was recrystallized by ethyl acetate. Yield 80% as white solid. ^{1}H NMR (400 MHz, $CDCl_3$) δ: 3.79 (s, 3H), 3.82 (t, 4H, J = 4.8 Hz), 4.19-4.48 (m, 4H), 7.67 (s, 1H). MS (ESI), m/z: 254.1 $[M+H]^+$.

2-chloro-9-methyl-6-morpholino-9*H*-purine-8-carbaldehyde (**4**). To a solution of **3** (2.53 g, 10 mmol, 1 equiv) in anhydrous THF (150 ml) at -78 ^{o}C under N_2 atmosphere was added TEMED (2.4 ml, 16 mmol, 1.6 equiv), followed by *n*-butyllithium (16 ml, 16 mmol, 1.6 equiv) dropwise. The reaction mixture was stirred for 30 min, then warmed to -40 ^{o}C for 1 h. DMF (1.5 ml, 20 mmol, 2.0 equiv) was added when the mixture was cooled to -78 ^{o}C and stirred for 2 h. The reaction was quenched with water, and the aqueous layer was extracted with CH_2Cl_2. The combined organic layers were dried over Na_2SO_4 and concentrated. The crude was not purified further. Yield, 51%. ^{1}H NMR (400 MHz, $CDCl_3$) δ: 3.79 (s, 3H), 3.92 (t, 4H, J = 4.8 Hz), 4.20-4.59 (m, 4H), 9.87 (s, 1H). MS (ESI), m/z: 282.1 $[M+H]^+$.

1-(2-chloro-9-methyl-6-morpholino-9*H*-purin-8-yl)-N-methylmethanamine (**5**). To a solution of **4** (4 g, 14 mmol, 1 equiv) in MeOH at 25 ^{o}C was added methylamine (25-30% in MeOH, 56 mmol) and stirred for 30 min, After the mixture was cooled to 0 ^{o}C, $NaBH_4$ (1.0 g, 28 mmol, 2 equiv) was added portionwise. Then the reaction mixture was warmed to 25 ^{o}C, and stirred for an additional 1 h. The solvent was removed under reduced pressure, extracted with water and CH_2Cl_2. The organic layer was separated and washed with saturated $NaHCO_3$ and brine. After dried over Na_2SO_4, the organic phase was concentrated to afford the desired crude **5**. The crude product was purified by flash chromatograph to yield **5** as white powder. ^{1}H NMR (400 MHz, DMSO-d_6) δ: 2.29 (s, 3H), 3.67 (s, 3H), 3.71 (t, 4H, J = 4.8 Hz), 3.85 (s, 1H), 4.02-4.30 (m, 4H). MS (ESI), m/z: 297.1 $[M+H]^+$.

Ethyl 2-(((2-chloro-9-methyl-6-morpholino-9*H*-purin-8-yl)methyl)(methyl)amino)pyrimidine-5-carboxylate (**7**). To a solution of **5** (296 mg, 1 mmol, 1 equiv) in CH_3CN at room temperature was added DIPEA (330 µl, 2 mmol, 2 equiv) and **6** (205.7 mg, 1.1 mmol, 1.1 equiv). About 2 h later, large amounts of precipitate came up. After filtration, the precipitate was obtained. Yield 81% as white powder. ^{1}H NMR (400 MHz, $CDCl_3$) δ: 1.38 (t, 3H, J = 7.2 Hz), 3.30 (s, 3H), 3.73 (s, 3H), 3.82 (t, 4H, J = 4.4 Hz), 4.18-4.40 (m, 4H), 4.36 (q, 2H, J = 7.2 Hz), 5.19 (s, 2H), 8.92 (s, 2H); MS (ESI), m/z: 447.2 $[M+H]^+$.

Ethyl 2-(methyl((9-methyl-6-morpholino-2-aryl-9*H*-purin-8-yl)methyl)amino)pyrimidine-5-

carboxylate (**9a−y**)**.** **7** (224 mg, 0.5 mmol, 1 equiv) was dissolved in toluene/ethanol/water (v:v:v, 7:3:2, 3 ml) and treated with **8** (0.6 mmol, 1.2 equiv), $PdCl_2(dppf)_2$, and $NaHCO_3$ (84 mg, 1 mmol, 2 equiv). The vial was sealed and heated with stirring at 80 ^oC for 8 h. The crude reaction mixture was purified by flash chromatograph to afford **9a−y**. Yield 70% as white powder.

N-hydroxy-2-(methyl((9-methyl-6-morpholino-2-phenyl-9*H*-purin-8-yl)methyl)amino)pyrimidine-5-carboxamide (**10a−y**). To a mixture of **9a−y** in CH_2Cl_2/CH_3OH (v:v, 1:1) at room temperature was added the solution of NH_2OH in CH_3OH. The reaction was stirred at room temperature for 2 h. The solution was quenched with water, then pH was adjusted to 7-8, and extracted with ethyl acetate. The solvent was removed under reduced pressure to afford the crude **10a−y** and purified by flash chromatograph. Yield, 90%.

N-hydroxy-2-(((2-chloro-9-methyl-6-morpholino-9*H*-purin-8-yl)methyl)(methyl)amino)pyrimidine-5-carboxamide (**10a**). **10a** was obtained from **9a** as described for method A. mp. 187-189 ^oC. ^1H NMR (400 MHz, DMSO-d_6) δ: 3.20 (s, 3H), 3.63-3.69 (m, 7H), 3.83-4.33 (m, 4H), 5.14 (s, 2H), 8.70 (s, 2H); HRMS (ESI), m/z: 447.1605 $[M+H]^+$.

N-hydroxy-2-(((2-(3-hydroxyphenyl)-9-methyl-6-morpholino-9*H*-purin-8-yl)methyl)(methyl)amino)pyrimidine-5-carboxamide (**10b**). **10b** was obtained from **9b** as described for method A. mp. 204-206 ^oC. ^1H NMR (400 MHz, DMSO-d_6) δ: 3.22 (s, 3H), 3.73-3.79 (m, 4H), 3.75 (s, 3H), 4.23-4.33 (m, 4H), 5.18 (s, 2H), 6.82 (s, 1H),

7.24-7.28 (m, 1H), 7.84-7.92 (m, 2H), 8.73 (s, 2H); HRMS (ESI), m/z: 492.2162 $[M+H]^+$.

N-hydroxy-2-(((2-(4-methoxyphenyl)-9-methyl-6-morpholino-*9H*-purin-8-yl)methyl)(methyl)amino)pyrimidine-5-carboxamide (**10c**). **10c** was obtained from **9c** as described for method A. mp. 191-193 ^oC. ^1H NMR (400 MHz, DMSO-d_6) δ: 3.23(s, 3H), 3.72-3.78(m, 4H), 3.75(s, 3H), 3.81 (s, 3H), 4.18-4.22 (m, 4H),5.17 (s, 2H), 7.01 (d, J = 8.8 Hz, 2H), 8.33 (d, J = 8.8 Hz, 2H), 8.72 (s, 2H), 9.03 (s, 1H), 11.09 (s, 1H); HRMS (ESI), m/z: 506.2328 $[M+H]^{+.}$

N-hydroxy-2-(methyl((9-methyl-6-morpholino-2-(3,4,5-trimethoxyphenyl)-9*H*-purin-8-yl)methyl)amino)pyrimidine-5-carboxamide (**10d**). **10d** was obtained from **9d** as described for method A. mp. 197-199 ^oC. ^1H NMR (400 MHz, DMSO-d_6) δ: 3.21 (s, 3H), 3.69-3.76 (m, 7H), 3.77 (s, 3H), 3.87 (s, 6H), 4.18-4.31 (m, 4H), 5.16 (s, 2H), 7.72 (s, 2H), 8.70 (s, 2H); HRMS (ESI), m/z: 566.2218 $[M+H]^+$.

N-hydroxy-2-(((2-(2-methoxy-5-(trifluoromethyl)phenyl)-9-methyl-6-morpholino-9*H*-purin-8-yl)methyl)(methyl)amino)pyrimidine-5-carboxamide (**10e**). **10e** was obtained from **9e** as described for method A. mp. 166-168 ^oC. ^1H NMR (400MHz, DMSO-d_6) δ: 3.22 (s, 3H), 3.58-3.64 (m, 4H), 3.70 (s, 3H), 3.84 (s, 3H), 4.11-4.21 (m, 4H), 5.18 (s, 2H), 7.30 (d, J = 8.8 Hz, 1H), 7.76 (d, J = 8.4 Hz, 1H), 7.80 (s, 1H), 8.71 (s, 2H); HRMS (ESI), m/z: 574.2054 $[M+H]^+$.

N-hydroxy-2-(methyl((9-methyl-6-morpholino-2-(4-(trifluoromethyl)phenyl)-9*H*-purin-8-yl)methyl)amino)pyrimidine-5-carboxamide (**10f**). **10f** was obtained from **9f** as described for method A. mp. 201-203 ^oC. ^1H NMR (400 MHz, DMSO-d_6) δ: 3.16

(s, 3H), 3.74 -3.77 (m, 7H), 4.21-4.32 (m, 4H), 5.16 (s, 2H), 7.82 (d, *J* = 8.4 Hz, 2H), 8.58 (d, *J* = 8.4 Hz, 2H), 8.64 (s, 2H); HRMS (ESI), m/z: 527.1817 $[M-H]^-$.

N-hydroxy-2-(((2-(3,5-bis(trifluoromethyl)phenyl)-9-methyl-6-morpholino-9*H*-purin-8-yl)methyl)(methyl)amino)pyrimidine-5-carboxamide (**10g**). **10g** was obtained from **9g** as described for method A. mp. 211-213 ^oC. ^1H NMR (400 MHz, DMSO-d_6) δ: 3.25 (s, 3H), 3.63-3.74 (m, 4H), 3.82 (s, 3H), 4.24-4.30 (m, 4H), 5.20 (s, 2H), 8.21 (s, 1H), 8.72 (s, 2H), 8.90 (s, 2H); HRMS (ESI), m/z: 612.2064 $[M+H]^+$.

N-hydroxy-2-(((2-(4-chloro-3-(trifluoromethyl)phenyl)-9-methyl-6-morpholino-9*H*-purin-8-yl)methyl)(methyl)amino)pyrimidine-5-carboxamide (**10h**). **10h** was obtained from **9h** as described for method A. mp. 197-199 ^oC. ^1H NMR (400 MHz, $CDCl_3$) δ: 3.30 (s, 3H), 3.81 (s, 3H), 3.83-3.91 (m, 4H), 4.26-4.40 (m, 4H), 7.55 (d, *J* = 8.4 Hz, 1H), 8.54 (d, *J* = 8.4 Hz, 1H), 8.77 (s, 2H), 8.95 (s, 1H); HRMS (ESI), m/z: 578.1648 $[M+H]^+$.

N-hydroxy-2-(((2-(benzo[d][1,3]dioxol-5-yl)-9-methyl-6-morpholino-9*H*-purin-8-yl)methyl)(methyl)amino)pyrimidine-5-carboxamide (**10i)**. **10i** was obtained from **9i** as described for method A. mp. 208-210 ^oC. ^1H NMR (400 MHz, DMSO-d_6) δ: 3.21 (s, 3H), 3.64-3.72 (m, 4H), 3.74 (s, 3H), 4.17-4.27 (m, 4H), 5.16 (s, 2H), 6.08 (s, 2H), 6.90 (d, *J* = 8.4 Hz, 1H), 7.87 (s, 1H), 7.99 (d, *J* = 8.4 Hz, 1H), 8.71 (s, 2H); HRMS (ESI), m/z: 520.2074 $[M+H]^+$.

N-hydroxy-2-(methyl((9-methyl-2-(4-(methylsulfonyl)phenyl)-6-morpholino-9*H*-purin-8-yl)methyl)amino)pyrimidine-5-carboxamide (**10j**). **10j** was obtained from **9j** as described for method A. mp. 213-215 ^oC. ^1H NMR (400 MHz, DMSO-d_6) δ: 3.25

(s, 6H), 3.70-3.77 (m, 4H), 3.79 (s, 3H), 4.20-4.35 (m, 4H), 5.20 (s, 2H), 8.02 (d, J = 8.0 Hz, 2H), 8.61 (d, J = 8.0 Hz, 2H), 8.73 (s, 2H); HRMS (ESI), m/z: 554.2016 $[M+H]^+$.

N-hydroxy-2-(methyl((9-methyl-6-morpholino-2-(p-tolyl)-9*H*-purin-8-yl)methyl) amino)pyrimidine-5-carboxamide (**10k**). **10k** was obtained from **9k** as described for method A. mp. 193-195 ^oC. ^1H NMR (400 MHz, DMSO-d_6) δ: 2.36 (s, 3H), 3.21 (s, 3H), 3.72 (s, 4H), 3.75 (s, 3H), 4.18-4.30 (m, 4H), 5.17 (s, 2H), 7.27 (d, J = 8.0 Hz, 2H), 8.29 (d, J = 8.0 Hz, 2H), 8.71 (s, 2H); HRMS (ESI), m/z: 490.2350 $[M+H]^+$.

N-hydroxy-2-(((2-(4-ethylphenyl)-9-methyl-6-morpholino-9*H*-purin-8-yl)methyl)(methyl)amino)pyrimidine-5-carboxamide (**10l**). **10l** was obtained from **9l** as described for method A. mp. 191-193 ^oC. ^1H NMR (400 MHz, DMSO-d_6) δ: 1.21 (t, J = 7.2 Hz, 3H), 2.66 (q, J = 7.2 Hz, 2H), 3.23 (s, 3H), 3.68-3.80 (m, 7H), 4.17-2.27 (m, 4H), 5.18 (s, 2H), 7.29 (d, J = 7.6 Hz, 2H), 8.30 (d, J = 7.6 Hz, 2H), 9.05 (s, 1H), 11.12 (s, 1H); HRMS (ESI), m/z: 504.2475 $[M+H]^+$.

N-hydroxy-2-(methyl((9-methyl-6-morpholino-2-(4-propylphenyl)-9*H*-purin-8-y l)methyl)amino)pyrimidine-5-carboxamide (**10m**). **10m** was obtained from **9m** as described for method A. mp. 172-174 ^oC. ^1H NMR (400 MHz, DMSO-d_6) δ: 0.92 (t, J = 7.2 Hz, 3H), 1.62 (m, J = 7.4 Hz, 2H), 2.60 (t, J = 7.5 Hz, 2H), 3.22 (s, 3H), 3.69-3.74 (m, 4H), 3.76 (s, 3H),4.17-4.27 (m, 4H), 5.18 (s, 2H), 7.28 (d, J = 8.0 Hz, 2H), 8.29 (d, J = 7.9 Hz, 2H), 8.72 (s, 2H); HRMS (ESI), m/z: 516.2615 $[M-H]^-$.

N-hydroxy-2-(((2-(4-(tert-butyl)phenyl)-9-methyl-6-morpholino-9*H*-purin-8-yl) methyl)(methyl)amino)pyrimidine-5-carboxamide (**10n**). **10n** was obtained from **9n**

as described for method A. mp. 198-200 °C. ^{1}H NMR (400 MHz, DMSO-d_6) δ: 1.32 (s, 9H), 3.23 (s, 3H), 3.67-3.75 (m, 4H), 3.76 (s, 3H), 4.17-4.29 (m, 4H), 5.18 (s, 2H), 7.48 (d, J = 8.4 Hz, 2H), 8.29 (d, J = 8.4 Hz, 2H), 8.73 (s, 2H), 9.06 (s, 1H), 11.12 (s, 1H); HRMS (ESI), m/z: 530.2073 $[M-H]^-$.

N-hydroxy-2-(((2-(4-aminophenyl)-9-methyl-6-morpholino-9*H*-purin-8-yl)methyl)(methyl)amino)pyrimidine-5-carboxamide (**10o**). **10o** was obtained from **9o** as described for method A. mp. 218-220 °C. ^{1}H NMR (400 MHz, DMSO-d_6) δ: 3.17 (s, 3H), 3.64-3.72 (m, 7H), 4.15-4.25 (m, 4H), 5.13 (s, 2H), 5.44 (s, 2H), 6.59 (d, J = 8.4 Hz, 2H), 8.09 (d, J = 8.4 Hz, 2H), 8.70 (s, 2H), 9.01 (s, 1H),11.2 (s, 1H); HRMS (ESI), m/z: 491.2105 $[M+H]^+$.

N-hydroxy-2-(((2-(4-(dimethylamino)phenyl)-9-methyl-6-morpholino-9*H*-purin-8-yl)methyl)(methyl)amino)pyrimidine-5-carboxamide (**10p**). **10p** was obtained from **9p** as described for method A. mp. 202-204 °C. ^{1}H NMR (400 MHz, DMSO-d_6) δ: 2.97 (s, 6H), 3.21 (s, 3H), 3.69 (m, 7H), 4.21 (m, 4H), 5.16 (s, 2H), 6.75 (d, J = 8.2 Hz, 2H), 8.22 (d, J = 8.2 Hz, 2H), 8.73 (s, 2H), 9.06 (s, 1H), 11.12 (s, 1H); HRMS (ESI), m/z: 519.2615 $[M+H]^+$.

N-hydroxy-2-(((2-(4-(ethylamino)phenyl)-9-methyl-6-morpholino-9*H*-purin-8-yl)methyl)(methyl)amino)pyrimidine-5-carboxamide (**10q**). **10q** was obtained from **9q** as described for method A. mp. 206-208 °C. ^{1}H NMR (400 MHz, DMSO-*d6*) δ: 1.18 (t, J = 7.2 Hz, 3H), 3.05-3.12 (q, J = 7.2 Hz, 2H), 3.21 (s, 3H), 3.67-3.75 (m, 7H), 4.15-4.26 (m, 4H), 5.16 (s, 2H), 5.53-5.66 (m, 1H), 6.59 (d, J = 8.8 Hz, 2H), 8.14 (d, J

= 8.8 Hz, 2H), 8.72 (s, 2H), 9.05(s, 1H), 11.11(s, 1H); HRMS (ESI), m/z: 517.2565 [M-H]$^-$.

N-hydroxy-2-(((2-(4-(bis(3-methylbut-2-en-1-yl)amino)phenyl)-9-methyl-6-morpholino-9*H*-purin-8-yl)methyl)(methyl)amino)pyrimidine-5-carboxamide (**10r**). **10r** was obtained from **9r** as described for method A. mp. 156-158 ^{o}C. ^{1}H NMR (400 MHz, DMSO-*d6*) δ: 1.70 (d, J = 3.6 Hz, 12H), 3.21 (s, 3H), 3.67-3.76 (m, 7H), 3.92 (d, J = 5.6 Hz, 4H), 414-4.26 (m, 4H), 5.12-5.20 (m, 4H), 6.68 (d, J = 8.8 Hz, 2H), 8.18 (d, J = 8.8 Hz, 2H), 8.73 (s, 2H), 9.05 (s, 1H), 11.10 (s, 1H); HRMS (ESI), m/z: 627.3517 [M+H]$^{+\cdot}$

N-hydroxy-2-(((2-(2-aminopyrimidin-5-yl)-9-methyl-6-morpholino-9*H*-purin-8-yl)methyl)(methyl)amino)pyrimidine-5-carboxamide (**10s**). **10s** was obtained from **9s** as described for method A. mp. 220-222 ^{o}C. ^{1}H NMR (400 MHz, DMSO-d_6) δ: 3.22 (s, 3H), 3.71-3.82 (m, 7H), 4.17-4.27 (m, 4H), 5.16 (s, H), 7.03 (s, 2H), 8.73 (s, 2H), 9.11 (s, 2H); HRMS (ESI), m/z: 491.2091 [M-H]$^-$.

N-hydroxy-2-(methyl((9-methyl-6-morpholino-2-(pyrimidin-5-yl)-9*H*-purin-8-yl)methyl)amino)pyrimidine-5-carboxamide (**10t**). **10t** was obtained from **9t** as described for method A. mp. 216-218 ^{o}C. ^{1}H NMR (400 MHz, DMSO-d_6) δ: 3.25 (s, 3H), 3.68-3.76 (m, 4H), 3.80 (s, 3H), 4.15-4.35 (m, 4H), 5.19 (s, 2H), 8.72 (s, 2H), 9.26 (s, 1H), 9.62 (s, 2H); HRMS (ESI), m/z: 476.2609 [M-H]$^-$.

N-hydroxy-2-(((2-(6-aminopyridin-3-yl)-9-methyl-6-morpholino-9*H*-purin-8-yl)methyl)(methyl)amino)pyrimidine-5-carboxamide (**10u**). **10u** was obtained from **9u** as described for method A. mp. 214-216 ^{o}C. ^{1}H NMR (400 MHz, DMSO-d_6) δ: 3.14

(s, 3H), 3.65-3.82 (m, 7H), 4.12-4.30 (m, 4H), 5.13 (s, 2H), 6.33 (s, 2H), 6.49 (d, *J* = 8.4 Hz, 1H), 8.29 (d, *J* = 8.4 Hz, 1H), 8.66 (s, 2H), 8.93 (s, 1H); HRMS (ESI), m/z: 492.2602 $[M+H]^+$.

N-hydroxy-2-(methyl((9-methyl-6-morpholino-2-(quinolin-3-yl)-9*H*-purin-8-yl) methyl)amino)pyrimidine-5-carboxamide (**10v**). **10v** was obtained from **9v** as described for method A. mp. 223-225 ^oC. ^1H NMR (400 MHz, DMSO-d_6) δ: 3.21 (s, 3H), 3.72-3.78 (m, 4H), 3.82 (s, 3H), 4.25-4.35 (s, 4H), 5.19 (s, 2H), 7.65 (t, *J* = 7.6 Hz, 1H), 7.80 (t, *J* = 7.6 Hz, 1H), 8.07 (d, *J* = 8.4 Hz, 1H), 8.16 (d, *J* = 8.0 Hz, 1H), 8.71 (s, 2H), 9.21 (s, 1H), 9.87 (s, 1H); HRMS (ESI), m/z: 527.2330 $[M+H]^+$.

N-hydroxy-2-(((2-(6-methoxypyridin-3-yl)-9-methyl-6-morpholino-9*H*-purin-8-yl)methyl)(methyl)amino)pyrimidine-5-carboxamide (**10w**). **10w** was obtained from **9w** as described for method A. mp. 192-194 ^oC. ^1H NMR (400 MHz, DMSO-d_6) δ: 3.23 (s, 3H), 3.68-3.74 (m, 4H), 3.76 (s, 3H), 3.92 (s, 3H), 4.18-4.28 (m, 4H), 5.17 (s, 2H), 6.91 (d, *J* = 8.4 Hz, 1H), 8.58 (d, *J* = 8.4 Hz, 1H), 8.72 (s, 2H), 9.14 (s, 1H); HRMS (ESI), m/z: 505.2260 $[M-H]^-$.

N-hydroxy-2-(methyl((9-methyl-6-morpholino-2-(pyridin-3-yl)-9*H*-purin-8-yl)methyl)amino)pyrimidine-5-carboxamide (**10x**). **10x** was obtained from **9x** as described for method A. mp. 217-219 ^oC. ^1H NMR (400 MHz, DMSO-d_6) δ: 3.23 (s, 3H), 3.68-3.75 (m, 4H), 3.79 (s, 3H), 4.17-4.32 (m, 4H), 7.45-7.51 (m, 1H), 8.60-8.68 (m, 2H), 8.72 (s, 2H), 9.53 (s, 1H); HRMS (ESI), m/z: 475.1937 $[M-H]^-$.

N-hydroxy-2-(methyl((9-methyl-6-morpholino-2-(pyridin-4-yl)-9*H*-purin-8-yl)methyl)amino)pyrimidine-5-carboxamide (**10y**). **10y** was obtained from **9y** as described

for method A. mp. 234-236 ^{o}C. ^{1}H NMR (400 MHz, DMSO-*d6*) δ: 3.24 (s, 3H), 3.72-3.78 (m, 4H), 3.80 (s, 3H), 4.16-4.32 (m, 4H), 5.20 (s, 2H), 8.26 (s, 2H), 8.71-8.78 (m, 4H), 9.05 (s, 1H), 11.07 (s, 1H); HRMS (ESI), m/z: 475.2047 $[M-H]^-$.

Biological Assay Methods

HDAC Enzymes Inhibition Assays. The HDAC activity of various compounds in vitro were performed by Chempartner company (Shanghai, China) with fluorigenic release of 7-amino-4-methylcoumarin (AMC) from substrate upon deacetylase enzymatic activity. Briefly, the release of AMC was promoted in the existence of trypsin. The compounds, diluted to the indicated concentrations, with full-length recombinant HDAC enzymes (BPS Biosciences), incubated at room temperature for 15 min, then followed by adding trypsin as well as Ac-peptide-AMC substrates, and the mixture was incubated at room temperature for 1 h. Reactions were performed in Tris-based assay buffer. The fluorescence measurements were obtained using a multilabel plate reader with excitation at 355 nm and emission at 460 nm. Data were analyzed on a plate-by-plate basis for the linear range of fluorescence over time. Wells containing recombinant HDAC, substrate and trypsin in the absence of small molecular inhibitors were set as control wells. Thus the data acquired from the groups containing the tested compounds were referred to the control wells. All of the designed groups, including controls, were run in duplicate. The data were finally fitted in GraphPad Prism V5.0 software to obtain IC_{50} values using equation (Y=Bottom + (Top-Bottom)/(1+10^((LogIC50-X)*Hill Slope), Y is %inhibition and X is compound concentration.).

PI3K Inhibition Assays. The PI3K activity assay was performed by Chempartner company (Shanghai, China). Briefly, diluted the compounds, PI3K enzyme (PI3Kα (p110α/p85a) from Invitrogen, PIK3Cβ (p110β) from Millipore, PIK3Cγ (pp110gamma) from Invitrogen, PIK3C δ (p110δ/p85a) from Millipore), PIP2 (life technologies) substrate and ATP (Sigma) in kinase buffer to the indicated concentrations, covered the assay plate and incubated at room temperature (PI3Kα, PI3Kβ and PI3Kγ for 1 h, PI3Kδ for 2 h). Then added the Kinase-Glo reagent (Promega) and incubated for 15 min in PI3Kα, PI3Kδ inhibition Assay. However, added the ADP-Gloreagen (Promega), incubated for 40 min, and followed by adding the Kinase Detection Reagent, shaked for 1 min, equilibrated for 1 h in PI3Kβ and PI3Kγ inhibition Assay. Collect data on Flex station. Data was presented in MS Excel and the curves fitted by GraphPad Prism V5.0.

Anti-proliferative Assays. A2780s, HCT116 cells were cultured in DMEM (Gibco, Milano, Italy) contained 10% fetal bovine serum (FBS) (Invitrogen, Milano, Italy). MV4-11cells were cultured in IMDM (Gibco, Milano, Italy) contained 10% fetal bovine serum (FBS) (Invitrogen, Milano, Italy). U266 cells were cultured in RPMI 1640 (Gibco, Milano, Italy) contained 15% fetal bovine serum (FBS) (Invitrogen, Milano, Italy). RPMI-8226, MM1S, OCI-LY1, HBL-1, Ramos, SUDHL-4, and Raji cells were cultured in RPMI 1640 (Gibco, Milano, Italy) containing 10% fetal bovine serum (FBS) (Invitrogen, Milano, Italy). All media contained 100 units/mL penicillin (Gibco, Milano, Italy), and 100 μg/mL streptomycin (Gibco, Milano, Italy). Cells were incubated at 37 ^{o}C in a humidified

atmosphere of 5% CO_2. Cells in logarithmic phase were seeded into 96-well culture plates at densities of (5000-10000) cells per well. After 24 h, cells were treated with various concentrations of compounds for 72 h in final volumes of 200 μL. Upon end point, 20 μL MTT (5 mg/mL) was added to each well, and the cells were incubated for an additional 1-3 h. After carefully removal of the medium, the precipitates were dissolved in DMSO, and then absorbance values at a wavelength of 570 nM were taken on a spectrophotometer (Molecular Devices, Sunnyvale, USA). IC_{50} values were calculated using percentage of growth versus untreated control.

HeLa Nuclear Extract HDAC inhibition assay. HeLa cells were cultured in DMEM (Gibco, Milano, Italy) containing 10% fetal bovine serum (FBS) (Invitrogen, Milano, Italy), 100 units/mL penicillin (Gibco, Milano, Italy) and 100 μg/mL streptomycin (Gibco, Milano, Italy). Cells were incubated at 37 ^{o}C in a humidified atmosphere of 5% CO_2. The nuclear extract was isolated via lysis (lysis buffer containing 50 mM Tris-HCl pH 7.4, 150 mM NaCl, 1% Triton x-100). The reaction mixture contains 25 mM Tris, pH 8.0, 1 mM $MgCl_2$, 0.1 mg/ml BSA, 1.37 mM NaCl, 2.7 mM KCl, HeLa extract and the enzyme substrate (20 μM Ac-Leu-Gly-Lys (Ac)-AMC). And the reactions were conducted at 37 ^{o}C for 30 min. After enzymatic reactions, 50 μL of 0.4 mg/ml Trypsin was added to each well and the plate was incubated at room temperature for an additional 15 min. The fluorescence measurements were obtained using a multilabel plate reader with excitation at 355 nm and emission at 460 nm. Wells absent of small molecular inhibitors were set as control wells. Thus the data acquired from the groups containing the tested compounds were

referred to the control wells. All of the designed groups, including controls, were run in duplicate. The data were finally fitted in GraphPad Prism V5.0 software to obtain IC_{50} values using equation (Y=Bottom + (Top-Bottom)/(1+10^((LogIC50-X)*Hill Slope), Y is %inhibition and X is compound concentration.).

***α*-Tubulin and Histone H3 Acetylation Cytoblot Assay.** The cytoblot assays were performed similarly as our previous work referring to the published method.[39, 40] Cells were seeded into opaque 96-well plates at a density of 5000 cells per well. After 24 h, the indicated concentrations of compounds were added and incubated for 6 h. Then cells were fixed with 3.7% paraformaldehyde in ice cold TBS at 4 ^{o}C for 1 h, permeabilized by −20 ^{o}C MeOH for 5 min at 4 ^{o}C and washed with 3% nonfat dry milk in TBS. The antiacetylated tubulin antibody (Santa Cruz), antiacetylated histone H_3 antibody (Santa Cruz) and horseradish peroxidase (HRP) conjugated secondary antibodies (Jackson) were added, and the plates were incubated for 4 h at 4 ^{o}C. After washing by TBS, the wells were added with enhanced chemiluminescence reagent and incubated for 5 min. Finally, the luminescence was measured by a Spectramax M5 microtiter plate luminometer. The software GraphPad Prism 5.0 was used to calculate the EC_{50} values.

Western Blotting. The cells were treated with the compounds at the indicated concentrations. Then the cells were collected and and total proteins were extracted with RIPA Lysis Buffer (beyotime Co. P0013B, components: 50 mM Tris, pH 7.4, 150 mM NaCl, 1% Triton X-100, 1% sodium deoxycholate, 0.1% SDS, 1 mM sodium orthovanadate, sodium fluoride, EDTA and leupeptin). The protein concentration was

measured by the BCA Protein assay (ThermoScientific, USA). Equivalent samples (20 μg of protein) were subjected to SDS-PAGE, and then the proteinswere transferred onto PVDF membranes (Millipore, USA). After blocking by 5% non-fat milk for 1 h at room temperature, the membranes were incubated with the indicated primary antibodies at 4 ^{o}C overnight and subsequently probed by the appropriate secondary antibodies conjugated to horseradish peroxidase for 1 h. Immunoreactive bands were visualized using enhanced chemiluminescence (Millipore, USA). The molecular sizes of the proteins detected were determined by comparison with pertained protein markers (ThermoScientific, USA).

Animal Tumor Models and Treatment. To establish the MV4-11 xenograft model, MV4-11 cells (10^7 cells in 100 μL serum-free IMDM) were injected subcutaneously into the right flanks of 5-6 week old female NOD/SCID mice. For the HCT116 xenograft, HCT116 cells (10^7 cells in 100 μL serum-free DMEM) were injected subcutaneously into the right flanks of 5-6 week old female Balb/c nude mice. As for MM1S and B cell lymphoma Ramos xenograft models, MM1S cells or Ramos cells (10^7 cells in 100 μL serum-free RPMI 1640) were injected subcutaneously into the right flanks of 5-6 week old female NOD/SCID mice. When the size of the formed xenografts reached 100-150 mm^3, the mice were randomly divided (6 mice per group in MV4-11 model, 6 mice per group in HCT116 model, 8 mice per group in Ramos model and 7 mice per group in MM1S model). In MV4-11, HCT116, Ramos and MM1S models, the mice in the experimental groups received intravenous injection (2, 5, 10 mg/kg, dissolved in physiological saline containing 20% captisol with the pH

adjusted to 6) of **10o** every 2 days, respectively. The mice in the vehicle group received iv injection equal amount of physiological saline 20% captisol with the pH adjusted to 6. Those in the SAHA group (positive control) received ip injection (50 mg/kg, dissolved in physiological saline containing 5% DMSO and 30% PEG400 to the concentration of 5 mg/ml) every 2 days. And the mice in the LBH-589 group (positive control) received ip injection (10 mg/kg, dissolved in physiological saline containing 2% DMSO, 2% Tween 80 and 15% PEG400 to the concentration of 1 mg/ml) every 2 days. Tumor burden was measured every 2 days by a caliper. Tumor volume (TV) was calculated using the following formula: TV =length × width^2 × 0.52. At the end of the experiment, mice were sacrificed and tumors were collected and weighed. The animal studies were conducted in conformity with institutional guide for the care and use of laboratory animals, and all mouse protocols were approved by the Animal Care and Use Committee of Sichuan University (Chengdu, Sichuan, China).

Pharmacokinetic study. A 2 mg/mL dosing solution of **10o** or **10o·CH_3SO_3H** was prepared by dissolving in physiological saline containing 20% captisol with the pH adjusted to 6 for iv administration and 0.5% CMC-Na aqueous solution for oral dosing, respectively. Ten SD rats, weighing 200−250 g each, were obtained from Beijing HFK Bioscience Co. Ltd. Five beagle dogs, weight 8-10 kg, each were kindly provided by Chengdu Center for GLP. Each tested compound was separately administered intravenously (5 mg/kg dose for rats or 6 mg/kg for beagle dogs) or orally (10 mg/kg for rats or 6 mg/kg for beagle dogs) to a group of five rats or dogs

per time. At time points 0 (prior to dosing), 5 min, 15 min, 30 min, 45 min, 1 h, 2 h, 4 h, 6 h, 8 h, 10 h, 12 h, and 24 h after dosing, a blood sample was collected from each animal via cardiac puncture and stored in ice (0 − 4 ^{o}C). Plasma was separated from the blood by centrifugation (4000 g for 15 min at 4 ^{o}C) and stored in a freezer at − 80 ^{o}C. All samples were analyzed for the tested compound by LC−MS/MS (Waters Acquity UPLC system; Waters Quattro Premier XE). Data were acquired via monitoring of multiple reactions. Plasma concentration data were analyzed by a standard noncompartmental method.

Molecular docking. Molecular docking studies were carried out to investigate the binding mode of compound **10o** and **10s** in the HDAC1 and PI3Kα, respectively. When compound **10s** was docked into the ATP pocket of PI3Kα isoform, the crystal structure in complex with a novel inhibitor (PDB code: 4L23[41)] was retrieved from the Protein Data Bank. And the molecular docking was completed by Autodock4.2[42]. Due to the specify of ubiquitous metalloenzyme which contain a zinc ion directly interacting with residues and inhibitors in HDAC1 binding site, FITTED 3.1[43], a docking software, which developing specific functions and parameters to account for zinc-drug coordination, was employed to accomplish the rational docking. In addition, since the crystal structure of HDAC1 obtained from HDAC1 in complex with the dimeric ELM2-SANT domain of MTA1 (PDB code: 4BKX[44]), the Flexible Docking implemented in Discovery Studio 3.1 was applied to the second round of docking. Finally, the best poses were kept and analyzed.

Associated content

Supporting information

General Procedures for the Synthesis of **18a−l**; Table S1 listing binding affinities of **10o** and **10s** with various Protein Kinases; Table S2 listing inhibition activities of **10o** against various tumor cell lines; Table S3 listing pharmacokinetic parameters of **10o**; Figure S1 showing structures of PI3Ks inhibitors; Figure S2 showing western blotting on HCT116 cell lines; Figure S3-4 showing molecular docking study. The Supporting Information is available free of charge via the Internet at http://pubs.acs.org.

PDB ID CODES

PDB code 4L23 was used for modeling docking in PI3Kα of compound **10o** and **10s**. PDB code 4BKX was used for modeling docking in HDAC1 of compound **10o** and **10s**. Authors will release the Atomic Coordinates and experimental data upon article publication.

Author information

Corresponding Author Information:

*To whom correspondence should be addressed: Lijuan Chen. Tel: +86-28-85164063; Fax: +86-28-85164060. E-mail address: chenlijuan125@163.com (L-j. Chen) or ljchen@scu.edu.cn.

Acknowledgement.

The authors greatly appreciate the financial support from National Key Programs of China during the 12th Five-Year Plan Period (2012ZX09103101-009) and National Natural Science Foundation of China (81373283).

Abbreviations Used: HDAC, histone deacetylase; PI3Ks, phosphatidylinositol

3-kinases; ZBG, zinc-binding group; MER, mitogen-activated protein kinase; SAHA, suberoylanilide hydroxamic acid; rt, room temperature; DIPEA, N,N-diisopropylethylamine; TEMED, N,N,N',N'-tetramethylethylenediamine; DMF, N,N-dimethylformamide; THF, tetrahydrofuran; SAR, structure−activity relationship; MTT, 3-(4,5-dimethylthiazol-2-yl)-2,5-diphenyltetrazolium bromide;

REFERENCES

1. Minucci, S.; Pelicci, P. G. Histone deacetylase inhibitors and the promise of epigenetic (and more) treatments for cancer. *Nat. Rev. Cancer* **2006**, *6*, 38-51.

2. Grunstein, M. Histone acetylation in chromatin structure and transcription. *Nature* **1997**, *389*, 349-352.

3. Struhl, K. Histone acetylation and transcriptional regulatory mechanisms. *Genes Dev.* **1998**, *12*, 599-606.

4. Wade, P. A. Transcriptional control at regulatory checkpoints by histone deacetylases: molecular connections between cancer and chromatin. *Hum. Mol. Genet.* **2001**, *10*, 693-698.

5. Wang, H.; Yu, N.; Chen, D.; Lee, K. C.; Lye, P. L.; Chang, J. W.; Deng, W.; Ng, M. C.; Lu, T.; Khoo, M. L.; Poulsen, A.; Sangthongpitag, K.; Wu, X.; Hu, C.; Goh, K. C.; Wang, X.; Fang, L.; Goh, K. L.; Khng, H. H.; Goh, S. K.; Yeo, P.; Liu, X.; Bonday, Z.; Wood, J. M.; Dymock, B. W.; Kantharaj, E.; Sun, E. T. Discovery of (2E)-3-{2-butyl-1-[2-(diethylamino)ethyl]-1H-benzimidazol-5-yl}-N-hydroxyacrylamide (SB939), an orally active histone deacetylase inhibitor with a superior preclinical profile. *J. Med. Chem.* **2011**, *54*, 4694-4720.

6. Gregoretti, I.; Lee, Y.-M.; Goodson, H. V. Molecular Evolution of the Histone Deacetylase Family: Functional Implications of Phylogenetic Analysis. *J. Mol. Biol.* **2004**, *338*, 17-31.

7. Kalin, J. H.; Bergman, J. A. Development and therapeutic implications of selective histone deacetylase 6 inhibitors. *J. Med. Chem.* **2013**, *56*, 6297-6313

8. Bradley E. Bernstein; Jeffrey K. Tong; Stuart L. Schreiber. Genomewide studies of histone deacetylase function in yeast. *Proc. Natl. Acad. Sci. U.S.A.* **2000**, *97*, 13708-13713.

9. Annemieke J.M., DE RUIJTER; Albert H., VAN GENNIP; CARON Huib N.; Stephan KEMP; Andre B.P. VAN KUILENBURG. Histone deacetylases(HDACs): Characterization of the classical HDAC family. *J. Bio. Chem.* **2003**, *370*, 737-749.

10. Leea, J.-H.; Yaob, Y.; Mahendranb, A.; Ngoa, L.; Venta-Pereza, G.; Choya, M. L.; Breslowb, R.; Marks, P. A. Creation of a histone deacetylase 6 inhibitor and its biological effects. *Proc. Natl. Acad. Sci. U.S.A.* **2015**, *112*, 12005-12010.

11. Foglietti C; Filocamo G; Cundari E; De Rinaldis E; Lahm A; Cortese R; Steinkuhler C. Dissecting the biological functions of drosophila histone deacetylases by RNA interference and transcriptional profiling. *J. Bio. Chem.* **2006**, *28*, 17968-17976.

12. Gryder, B. E.; Sodji, Q. H.; Oyelere, A. K. Targeted cancer therapy: giving histone deacetylase inhibitors all they need to succeed. *Future Med. Chem.* **2012**, *4*, 505-524.

13. Duvic, M.; Talpur, R.; Ni, X.; Zhang, C.; Hazarika, P.; Kelly, C.; Chiao, J. H.;

Reilly, J. F.; Ricker, J. L.; Richon, V. M.; Frankel, S. R. Phase 2 trial of oral vorinostat (suberoylanilide hydroxamic acid, SAHA) for refractory cutaneous T-cell lymphoma (CTCL). *Blood* **2007**, *109*, 31-39.

14. Butler, L. M.; Zhou, X.; Xu, W. S.; Scher, H. I.; Rifkind, R. A.; Marks, P. A.; Richon, V. M. The histone deacetylase inhibitor SAHA arrests cancer cell growth, up-regulates thioredoxin-binding protein-2, and down-regulates thioredoxin. *Proc. Natl. Acad. Sci. U.S.A.* **2002**, *99*, 11700-11705.

15. Atadja, P. Development of the pan-HDAC inhibitor panobinostat (LBH589): successes and challenges. *Cancer Lett.* **2009**, *280*, 233-41.

16. Ahmed Sawas; Dejan Radeski; Owen A. O'Connor. Belinostat in patients with refractory or relapsed peripheral T-cell lymphoma: a perspective review. *Ther. Adv. Hematol.* **2015**, *6*, 202 –208.

17. Zorzi, A. P.; Bernstein, M.; Samson, Y.; Wall, D. A.; Desai, S.; Nicksy, D.; Wainman, N.; Eisenhauer, E.; Baruchel, S. A phase I study of histone deacetylase inhibitor, pracinostat (SB939), in pediatric patients with refractory solid tumors: IND203 a trial of the NCIC IND program/C17 pediatric phase I consortium. *Pediatr. Blood Cancer* **2013**, *60*, 1868-1874.

18. Gore, L.; Rothenberg, M. L. ;O'Bryant, C. L.; Schultz, M. K.; Sandler, A. B.; Coffin, D.; McCoy, C.; Schott, A.; Scholz, C.; Eckhardt, S. G. A phase I and pharmacokinetic study of the oral histone deacetylase inhibitor, MS-275, in patients with refractory solid tumors and lymphomas. *Clin. Cancer Res*. **2008**, *14*, 4517-4525.

19. Haggarty, S. J.; Koeller, K. M.; Wong, J. C.; Grozinger, C. M.; Schreiber, S. L.

Domain-selective small-molecule inhibitor of histone deacetylase 6 (HDAC6) –mediated tubulin deacetylation. *Proc. Natl. Acad. Sci. U.S.A.* **2003**, *100*, 4389-4394.

20. Haggarty, S. J.; Koeller, K. M.; Wong, J. C.; Butcher, R. A.; Schreiber, S. L. Multidimensional chemical genetic analysis of diversity-oriented synthesis –derived deacetylase inhibitors using cell-based assays. *Chem. Biol.* **2003**, *10*, 383-396.

21. Heffron, T. P.; Salphati, L.; Alicke, B.; Cheong, J.; Dotson, J.; Edgar, K.; Goldsmith, R.; Gould, S. E.; Lee, L. B.; Lesnick, J. D.; Lewis, C.; Ndubaku, C.; Nonomiya, J.; Olivero, A. G.; Pang, J.; Plise, E. G.; Sideris, S.; Trapp, S.; Wallin, J.; Wang, L.; Zhang, X. The design and identification of brain penetrant inhibitors of phosphoinositide 3-Kinase α. *J. Med. Chem.* **2012**, *55*, 8007-8020.

22. Sutherlin, D. P.; Bao, L.; Berry, M.; Castanedo, G.; Chuckowree, I.; Dotson, J.; Folks, A.; Friedman, L.; Goldsmith, R.; Gunzner, J.; Heffron, T.; Lesnick, J.; Lewis, C.; Mathieu, S.; Murray, J.; Nonomiya, J.; Pang, J.; Pegg, N.; Prior, W. W.; Rouge, L.; Salphati, L.; Sampath, D.; Tian, Q.; Tsui, V.; Wan, N. C.; Wang, S.; Wei, B.; Wiesmann, C.; Wu, P.; Zhu, B. Y.; Olivero, A. Discovery of a potent, selective, and orally available class I phosphatidylinositol 3-kinase (PI3K)/mammalian target of rapamycin (mTOR) kinase inhibitor (GDC-0980) for the treatment of cancer. *J. Med. Chem.* **2011**, *54*, 7579-7587.

23. Saurat, T.; Buron, F.; Rodrigues, N.; de Tauzia, M. L.; Colliandre, L.; Bourg, S.; Bonnet, P.; Guillaumet, G.; Akssira, M.; Corlu, A.; Guillouzo, C.; Berthier, P.; Rio, P.; Jourdan, M. L.; Benedetti, H.; Routier, S. Design, synthesis, and biological activity of pyridopyrimidine scaffolds as novel PI3K/mTOR dual inhibitors. *J. Med. Chem.*

2014, 57, 613-631.

24. Liu, P. X.; Cheng, H. L.; Roberts, T. M.; Zhao, J. J. Targeting the phosphoinositide 3-kinase pathway in cancer. *Nat. Rev. Drug Discovery* **2009**, *8*, 627-644.

25. Folkes, A. J.; Ahmadi, K.; Alderton, W. K.; Alix, S.; Baker, S. J.; Box, G.; Chuckowree, I. S.; Clarke, P. A.; Depledge, P.; Eccles, S. A.; Friedman, L. S.; Hayes, A.; Hancox, T. C.; Kugendradas, A.; Lensun, L.; Moore, P.; Olivero, A. G.; Pang, J.; Patel, S.; Pergl-Wilson, G. H.; Raynaud, F. I.; Robson, A.; Saghir, N.; Salphati, L.; Sohal, S.; Ultsch, M. H.; Valenti, M.; Wallweber, H. J. A.; Wan, N. C.; Wiesmann, C.; Workman, P.; Zhyvoloup, A.; Zvelebil, M. J.; Shuttleworth, S. J. The identification of 2-(1H-Indazol-4-yl)-6-(4-methanesulfonyl-piperazin-1-ylmethyl)-4–morpholin-4-yl-thieno[3,2-d]pyrimidine (GDC-0941) as a potent, selective, orally bioavailable inhibitor of class I PI3 kinase for the treatment of cancer. *J. Med. Chem.* **2008**, *51*, 5522-5532.

26. Heald, R. A.; Jackson, P.; Savy, P.; Jones, M.; Gancia, E.; Burton, B.; Newman, R.; Boggs, J.; Chan, E.; Chan, J.; Choo, E.; Merchant, M.; Rudewicz, P.; Ultsch, M.; Wiesmann, C.; Yue, Q.; Belvin, M.; Price, S. Discovery of novel allosteric mitogen-activated protein kinase kinase (MEK) 1,2 inhibitors possessing bidentate Ser212 interactions. *J. Med. Chem.* **2012**, *55*, 4594-4604.

27. Burger, M. T.; Pecchi, S.; Wagman, A.; Ni, Z. J.; Knapp, M.; Hendrickson, T.; Atallah, G.; Pfister, K.; Zhang, Y.; Bartulis, S.; Frazier, K.; Ng, S.; Smith, A.;

Verhagen, J.; Haznedar, J.; Huh, K.; Iwanowicz, E.; Xin, X.; Menezes, D.; Merritt, H.; Lee, I.; Wiesmann, M.; Kaufman, S.; Crawford, K.; Chin, M.; Bussiere, D.; Shoemaker, K.; Zaror, I.; Maira, S. M.; Voliva, C. F. Identification of NVP-BKM120 as a potent, selective, orally bioavailable class I PI3 kinase inhibitor for treating Cancer. *ACS Med. Chem. Lett.* **2011**, *2*, 774-779.

28. Salphati, L.; Heffron, T. P.; Alicke, B.; Nishimura, M.; Barck, K.; Carano, R. A.; Cheong, J.; Edgar, K. A.; Greve, J.; Kharbanda, S.; Koeppen, H.; Lau, S.; Lee, L. B.; Pang, J.; Plise, E. G.; Pokorny, J. L.; Reslan, H. B.; Sarkaria, J. N.; Wallin, J. J.; Zhang, X.; Gould, S. E.; Olivero, A. G.; Phillips, H. S. Targeting the PI3K pathway in the brain-efficacy of a PI3K inhibitor optimized to cross the blood-brain barrier. *Clin. Cancer Res.* **2012**, *18*, 6239-6248.

29. Salphati, L.; Shahidi-Latham, S.; Quiason, C.; Barck, K.; Nishimura, M.; Alicke, B.; Pang, J.; Carano, R. A.; Olivero, A. G.; Phillips, H. S. Distribution of the phosphatidylinositol 3-kinase inhibitors Pictilisib (GDC-0941) and GNE-317 in U87 and GS2 intracranial glioblastoma models-assessment by matrix-assisted laser desorption ionization imaging. *Drug Metab. Dispos.* **2014**, *42*, 1110-1116.

30. Qian, C.; Lai, C. J.; Bao, R.; Wang, D. G.; Wang, J.; Xu, G. X.; Atoyan, R.; Qu, H.; Yin, L.; Samson, M.; Zifcak, B.; Ma, A. W.; DellaRocca, S.; Borek, M.; Zhai, H. X.; Cai, X.; Voi, M. Cancer network disruption by a single molecule inhibitor targeting both histone deacetylase activity and phosphatidylinositol 3-kinase signaling. *Clin. Cancer Res.* **2012**, *18*, 4104-4113.

31. Kolev, V. N.; Wright, Q. G.; Vidal, C. M.; Ring, J. E.; Shapiro, I. M.; Ricono, J.;

Weaver, D. T.; Padval, M. V.; Pachter, J. A.; Xu, Q. PI3K/mTOR dual inhibitor VS-5584 preferentially targets cancer stem cells. *Cancer Res.* **2015**, *75*, 446-455.

32. Puri, K. D.; Steiner, B. H.; Kashishian, A. S.; Chen, H.; Gallatin, W. M.; Giese, N. A. IC87114, a selective inhibitor of PI3K δ suppresses joint inflammation and bone erosion in collagen-induced arthritis in rat. *J. Immunol.* **2009**, *182*, 50.14.

33. Li, J.; Hou, N.; Faried, A.; Tsutsumi, S.; Takeuchi, T.; Kuwano, H. Inhibition of autophagy by 3-MA enhances the effect of 5-FU-induced apoptosis in colon cancer cells. *Ann. Surg. Oncol.* **2008**, *16*, 761-771.

34. Andrs, M.; Korabecny, J.; Jun, D.; Hodny, Z.; Bartek, J.; Kuca, K. Phosphatidylinositol 3-Kinase (PI3K) and phosphatidylinositol 3-kinase-related kinase (PIKK) inhibitors: importance of the morpholine ring. *J. Med. Chem.* **2015**, *58*, 41-71.

35. Remiszewski, S. W.; Sambucetti, L. C.; Bair, K. W.; Bontempo, J.; Cesarz, D.; Chandramouli, N.; Chen, R.; Cheung, M.; Cornell-Kennon, S.; Dean, K.; Diamantidis, G.; France, D.; Green, M. A.; Howell, K. L.; Kashi, R.; Kwon, P.; Lassota, P.; Martin, M. S.; Mou, Y.; Perez, L. B.; Sharma, S.; Smith, T.; Sorensen, E.; Taplin, F.; Trogani, N.; Versace, R.; Walker, H.; Weltchek-Engler, S.; Wood, A.; Wu, A.; Atadja, P. N-Hydroxy-3-phenyl-2-propenamides as novel inhibitors of human histone deacetylase with in vivo antitumor activity: discovery of (2E)-N-Hydroxy-3-[4-[[(2-hydroxyethyl)[2-(1H-indol-3-yl)ethyl]amino]methyl]-phen yl]-2-propenamide (NVP-LAQ824). *J. Med. Chem.* **2003**, *46*, 4609-4624.

36. Plumb, J. A.; Finn, P. W.; Williams, R. J.; Bandara, M. J.; Romero, M. R.;

Watkins, C. J.; Thangue, N. B. L.; Brown, R. Pharmacodynamic response and inhibition of growth of human tumor xenografts by the novel histone deacetylase inhibitor PXD101. *Mol. Cancer Ther.* **2003**, *2*, 721-728.

37. Yeo, P.; Xin, L.; Goh, E.; New, L. S.; Zeng, P.; Wu, X.; Venkatesh, P.; Kantharaj, E. Development and validation of high-performance liquid chromatography–tandem mass spectrometry assay for 6-(3-benzoyl-ureido)-hexanoic acid hydroxyamide, a novel HDAC inhibitor, in mouse plasma for pharmacokinetic studies. *Biomed. Chromatogr.* **2007**, *21*, 184-189.

38. Khochbin, S.; Verdel, A.; Lemercier, C.; Seigneurin-Berny, D. Functional significance of histone deacetylase diversity. *Curr. Opin. Genet. Dev.* **2001**, *11*, 162-166.

39. Tang, G.; Wong, J. C.; Zhang, W.; Wang, Z.; Zhang, N.; Peng, Z.; Zhang, Z.; Rong, Y.; Li, S.; Zhang, M.; Yu, L.; Feng, T.; Zhang, X.; Wu, X.; Wu, J. Z.; Chen, L. Identification of a novel aminotetralin class of HDAC6 and HDAC8 selective inhibitors. *J. Med. Chem.* **2014**, *57*, 8026-8034.

40. Yang, Z.; Wang, T.; Niu, F. W. T.; Liu, Z.; Chen, X.; Long, C.; Tang, M.; Cao, D.; Wang, X.; Xiang, W.; Yi, Y.; Ma, L.; You, J.; Chen, L. Discovery of selective histone deacetylase 6 inhibitors using the quinazoline as the cap for the treatment of cancer. *J. Med. Chem.* **2016**, *59*, 1455-1470.

41. Zhao, Y.; Zhang, X.; Chen, Y.; Lu, S.; Peng, Y.; Wang, X.; Guo, C.; Zhou, A.; Zhang, J.; Luo, Y.; Shen, Q.; Ding, J.; Meng, L.; Zhang, J. Crystal structures of PI3K alpha complexed with PI103 and its derivatives: new directions for inhibitors design.

ACS Med. Chem. Lett. **2014**, *5*, 138-142.

42. Morris, G. M.; Huey, R.; Lindstrom, W.; Sanner, M. F.; Belew, R. K.; Goodsell, D. S.; Olson, A. J. AutoDock4 and AutoDockTools4: Automated docking with selective receptor flexibility. *J. Comput. Chem.* **2009**, *30*, 2785-2791.

43. Pottel, J.; Therrien, E.; Gleason, J. L.; Moitessier, N. Docking ligands into flexible and solvated macromolecules. 6. Development and application to the docking of HDACs and other zinc metalloenzymes inhibitors. *J. Chem. Inf. Model.* **2014**, *54*, 254-265.

44. Millard, Christopher J.; Watson, Peter J.; Celardo, I.; Gordiyenko, Y.; Cowley, Shaun M.; Robinson, Carol V.; Fairall, L.; Schwabe, John W. R. Class I HDACs share a common mechanism of regulation by inositol phosphates. *Molecular Cell* **2013**, *51*, 57-67.

Table of Contents Graphic

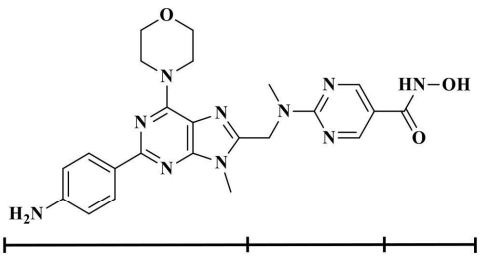

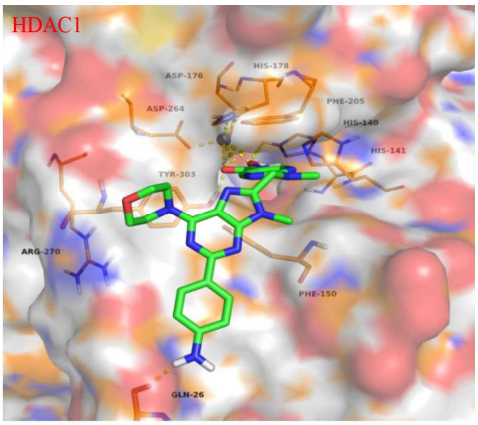

HDAC1 = 1.00 nM , HDAC6 = 4.65 nM;

Antiproliferative activity IC_{50}s = 0.15~12.85 nM;

Oral bioavailability F= 41.82% (dogs, mesylate).